Neurobiology of Disease

Stabilization of Nontoxic Aβ-Oligomers: Insights into the Mechanism of Action of Hydroxyquinolines in Alzheimer's Disease

Timothy M. Ryan,[1]* **Blaine R. Roberts,**[1]* **Gawain McColl,**[1]* **Dominic J. Hare,**[1,2] **Philip A. Doble,**[2] **Qiao-Xin Li,**[1] **Monica Lind,**[1] **Anne M. Roberts,**[1] **Haydyn D. T. Mertens,**[3] **Nigel Kirby,**[3] **Chi L. L. Pham,**[4] **Mark G. Hinds,**[5,6] **Paul A. Adlard,**[1] **Kevin J. Barnham,**[1,4,5] **Cyril C. Curtain,**[1] and **Colin L. Masters**[1]

[1]Florey Institute of Neuroscience and Mental Health, University of Melbourne, Parkville 3052, Victoria, Australia, [2]Elemental Bio-imaging Facility, University of Technology Sydney, Broadway 2007, New South Wales, Australia, [3]Australian Synchrotron, Clayton 3168, Victoria, Australia, [4]Department of Pharmacology, University of Melbourne, Parkville 3052, Victoria, Australia, [5]Bio21 Molecular Science and Technology Institute, University of Melbourne, Parkville 3052, Victoria, Australia, and [6]School of Chemistry, University of Melbourne, Parkville 3052, Victoria, Australia

The extracellular accumulation of amyloid β (Aβ) peptides is characteristic of Alzheimer's disease (AD). However, formation of diffusible, oligomeric forms of Aβ, both on and off pathways to amyloid fibrils, is thought to include neurotoxic species responsible for synaptic loss and neurodegeneration, rather than polymeric amyloid aggregates. The 8-hydroxyquinolines (8-HQ) clioquinol (CQ) and PBT2 were developed for their ability to inhibit metal-mediated generation of reactive oxygen species from Aβ:Cu complexes and have both undergone preclinical and Phase II clinical development for the treatment of AD. Their respective modes of action are not fully understood and may include both inhibition of Aβ fibrillar polymerization and direct depolymerization of existing Aβ fibrils. In the present study, we find that CQ and PBT2 can interact directly with Aβ and affect its propensity to aggregate. Using a combination of biophysical techniques, we demonstrate that, in the presence of these 8-HQs and in the absence of metal ions, Aβ associates with two 8-HQ molecules and forms a dimer. Furthermore, 8-HQ bind Aβ with an affinity of 1–10 μM and suppress the formation of large (>30 kDa) oligomers. The stabilized low molecular weight species are nontoxic. Treatment with 8-HQs also reduces the levels of *in vivo* soluble oligomers in a *Caenorhabditis elegans* model of Aβ toxicity. We propose that 8-HQs possess an additional mechanism of action that neutralizes neurotoxic Aβ oligomer formation through stabilization of small (dimeric) nontoxic Aβ conformers.

Key words: Alzheimer's disease; amyloid beta peptide; hydroxyquinoline; oligomer; PBT2; toxicity

Introduction

Alzheimer's disease (AD) is characterized by the accumulation of the amyloid-β (Aβ) peptide within the extracellular space of the brain (Masters et al., 1985; Kang et al., 1987). Although these deposits of Aβ are the pathognomonic feature of AD, the degree

of synaptic loss correlates more with the soluble/diffusible species of Aβ oligomers (Lambert et al., 1998), which in turn are in equilibrium with insoluble Aβ aggregates (Mawuenyega et al., 2010). This has led to the soluble oligomer theory of AD, where a specific small, diffusible Aβ oligomer causes synaptic damage beyond the brain's repair capacity. This theory has been supported by the finding of SDS-stable dimers in human brain tissue, which affect LTP (Shankar et al., 2008), and the observation that levels of a 56 kDa oligomer (labeled Aβ 56*) correlate with the severity of cognitive dysfunction (Lesné et al., 2006). There are many different methods for generating toxic oligomers *in vitro* (for review, see Benilova et al., 2012), which lead to a corresponding array of numerous oligomeric forms of Aβ, with little evidence of which *in vitro* configurations actually exist *in vivo*, or are specific to disease pathogenesis (for reviews, see Hayden and Teplow, 2013; Ryan et al., 2013b). Despite this uncertainty, assays of these oligomers and development of antibodies targeting the Aβ peptide have been a major theme in the recent efforts to develop a therapy for AD (Imbimbo et al., 2012; Tayeb et al., 2013).

Clioquinol (CQ; 5-chloro-7-iodo-quinolin-8-ol; Fig. 1A, inset), a first-generation metal-protein attenuating compound and

2-(dimethylamino)methyl-5,7-dichloro-8-hydroxyquinoline (PBT2; Figure 1A, inset) (Telpoukhovskaia et al., 2014), a second-generation metal-protein attenuating compound that crosses the blood–brain barrier (Padmanabhan et al., 1989; Adlard et al., 2008), are examples of alternative approaches to targeting Aβ in the brain. This approach uses small molecules directed toward inhibiting aberrant interactions of metals (e.g., Cu and Zn) and Aβ. PBT2 has successfully completed two Phase II clinical trials in AD, the first of which has shown PBT2 to have significant positive effects on cognition with concomitant reduction in CSF Aβ levels (Lannfelt et al., 2008; Faux et al., 2010). The results of the second Phase II trial are currently being evaluated.

The initial proposed mechanisms of action for PBT2 and CQ include a metal chaperone activity, inhibiting reactive oxygen species generated from Aβ:Cu complexes, inhibition of dityrosine cross-links, disaggregation of Aβ amyloid fibrils, and promoting uptake of metals by cells (Cherny et al., 2001; White et al., 2006; Adlard et al., 2008; Bush, 2008; Crouch et al., 2011). Two current studies have implicated the formation of ternary complexes between 8-hydroxyquinoline (8-HQ), Aβ, and a divalent metal cation in the proposed mechanism of action (Kenche et al., 2013; Matlack et al., 2014). It has also been observed that 8-HQs affect the aggregation of a range of proteins, including the Aβ peptide (LeVine et al., 2009; Cheng et al., 2012), Huntingtin polyglutamine, TDP-43, and α-synuclein (Tardiff et al., 2012) with no addition of exogenous metal ions. The direct, metal-independent interaction of 8-HQs with Aβ may provide an additional mechanism of action (LeVine et al., 2009). Here we investigated the effect of these compounds on oligomerization of Aβ under metal-free conditions. The *in vivo* effects of CQ and PBT2 were also explored on a *Caenorhabditis elegans* model of Aβ toxicity, showing that hydroxyquinoline treatment results in a change in the *in vivo* oligomeric status of Aβ.

Materials and Methods

Human and mouse Aβ1–42 was synthesized by the W. M. Keck Laboratory (Yale University, New Haven, CT) and its purity confirmed by high performance liquid chromatography (HPLC) and mass spectrometry, which indicated no significant oxidation or modification. *N*-terminally fluorescein-tagged Aβ was synthesized in-house using standard Fmoc chemistry. Peptide identity and purity were confirmed by reverse-phase HPLC and mass spectrometry. PBT2 was kindly donated by Prana Biotechnology. CQ was purchased from Sigma (catalog #33931-100MG-R). Solutions of both 8-HQs, PBS, Tris-HCl buffered saline, and water used for buffer preparation were confirmed to be metal free ($\ll 0.03 \mu$M), with inductively coupled plasma mass spectrometry (ICPMS). All other reagents were of analytical grade.

Aβ1–42 preparation. Aβ1–42 was resuspended using a sodium hydroxide-based protocol as described previously (Ryan et al., 2013a). Briefly, 1 mg of peptide was resuspended in 200 μl of 60 mM NaOH and incubated for 5 min at room temperature. This solution was diluted with 700 μl of distilled water and bath sonicated at room temperature for a further 5 min. The sonicated solution was neutralized with 100 μl of 10× PBS, pH 7 (50 mM sodium phosphate, 150 mM sodium chloride) and centrifuged at $14,000 \times g$. The optical density at 214 nm of the supernatant, containing the resolubilized Aβ1–42, was determined with a quartz microplate and a Flexstation 3 plate reader (Molecular Devices) equipped with absorbance optics. The concentration was calculated from the absorbance value at 214 nm using an extinction coefficient for Aβ1–42 of $95,452 \text{ M}^{-1} \text{ cm}^{-1}$ (McColl et al., 2009). Peptide purity was determined using matrix-assisted laser desorption/ionization-time of flight-mass spectrometry (MALDI-TOF MS; Bruker). Recovery of Aβ1–42 was typically 60%–80% based on dry weight of the peptide.

Thioflavin T (ThT) assays. The effect of PBT2 on the aggregation of Aβ1–42 was measured using a continuous ThT fluorescence assay described previously (McColl et al., 2009; Ryan et al., 2012, 2013a). PBT2/CQ was prepared as a 1 mM stock in DMSO, and diluted into PBS containing ThT (10 μM) to a final concentration of 10 μM. Aβ1–42 was added to a final concentration of 5 μM, and the plate was incubated at 37°C, with shaking every 7 min, for 3 s, before the measurement of the ThT fluorescence intensity (444 nm excitation and 485 nm emission), using a Flexstation 3 Plate reader. All measurements were conducted in triplicate and averaged, and the experiment was repeated 4 times independently, with different reagent batches. Controls where DMSO alone was added were also conducted.

In addition, point-based-ThT measures were acquired to determine 50% inhibitory concentrations (IC$_{50}$ values) and the effect of the 8-HQ on preformed fibrils. To determine IC$_{50}$ values, a series of solutions (in triplicate) were prepared in 1.5 ml microcentrifuge tubes comprising 5 μM Aβ in PBS, pH 7.4, supplemented with 0, 0.8, 1.6, 3.25, 7.5, 10, or 15 μM of PBT2/CQ, and 10 μM ThT. These solutions were incubated at 37°C with shaking. After 24 h, 100 μl aliquots were transferred to 96 well plates and the ThT fluorescence intensity (444 nm excitation, 485 nm emission) was measured in triplicate with the Flexstation 3 plate reader.

To investigate the effect of 8-HQs on preformed fibrils, Aβ peptides (5 μM) were incubated in 1 ml of PBS, 10 μM ThT for 24 h at 37°C with shaking. Increased ThT fluorescence, suggesting the presence of fibrils, was confirmed using the above point-based assay. PBT2 and CQ were added to a final concentration of 10 μM, by adding 1 μl of a 1 mM stock solution per 100 μl of sample. Controls, where the equivalent amount of DMSO was added, were also prepared. The solutions were incubated at 37°C with no shaking and periodically measured by the above point-based assay.

Further analysis was conducted by centrifuging 100 μl of Aβ1–42 solutions incubated with the 8-HQs (after 24 h) or solutions where hydroxyquinolines were added to preformed fibrils at $100,000 \times g$ for 30 min, and then quantifying the protein levels of the supernatant and pellet with a BCA assay (Pierce). All measurements were performed in triplicate.

Electron microscopy. Solutions from the continuous aggregation assays were vortexed to suspend particulate matter, and an aliquot was spotted onto carbon-coated copper grids (ProSciTech). The grids were washed several times with distilled water to remove excess phosphate and then allowed to air dry. The fibrils were negatively stained with 0.5% uranyl acetate for 3 min and then washed several times with water. The samples were analyzed on a Siemens ELMIS-KOP 102 electron microscope. The films were scanned using a flatbed scanner and the resulting image saved as a tiff file. These experiments were conducted in triplicate, from three different experiments. Twenty images were taken across all grids to ensure that the selected images were representative of the sample.

Analytical ultracentrifugation experiments. Sedimentation experiments were conducted at a concentration of 15 μM Aβ1–42 using an XL-I analytical ultracentrifuge (Beckman Coulter). Sedimentation velocity measurements were performed at 50,000 rpm and 20°C, using centrifuge cells equipped with quartz windows and charcoal epon dual-sector centerpieces and a sample volume of 300 μl. The sedimentation velocity of the 8-HQ compounds at various ratios with Aβ1–42, solubilized and prepared as described above using PBS as the buffering solution, was investigated by acquiring a radial 350 nm absorbance scan every 7 min.

Sedimentation velocity analysis of Aβ1–42 was measured specifically by using fluorescein-labeled Aβ, which was detected using a Fluorescence Detection System (Aviv Biomedicals), which constitutes a 488 nm excitation laser and detection of fluorescence emission via a photomultiplier tube equipped with a 505 nm long-pass filter. With this system, the fluorescence intensity of 15 μM Aβ1–42 peptide spiked with 1 nM *N*-terminally fluorescein-labeled Aβ1–42 in the presence and absence of 15 μM 8-HQ was acquired as a function of radial position every 2 min for the duration of the experiment. All velocity data were analyzed using a continuous sedimentation coefficient distribution model [c(S)] and the program SEDFIT version 9.4 (Schuck, 2000, 2003). The amount of sedimenting compound was assessed after baseline correction by taking the average of the first 10 data points of the first scan of the run (total optical density) and subtracting the average of the first 10 points of the final scan (change in optical density). This was expressed as a proportion by divid-

ing the by total optical density and was plotted as function of 8-HQ concentration. The weight average sedimentation coefficient (*Sw*) was assessed by integrating the c(S) distributions provided by SEDFIT, and this value was also plotted as a function of PBT2 concentration.

Sedimentation equilibrium analysis was also performed. In contrast to the sedimentation velocity, only 100 μl of sample was loaded into the centrifuge cells. Samples were spun at 26,000, 36,000, and 46,000 rpm, and the concentration gradient formed over time at these speeds was monitored using the absorbance at 230 nm. When the samples had reached equilibrium (i.e., there was no change in the concentration gradient over a period of 4 h), a high-quality scan was acquired, using a step size of 10 μm and averaging of 10 separate scans at 230 nm. With this wavelength, there was a significant contribution of the compound absorbance. Data were analyzed using SedPHAT (Vistica et al., 2004) with a model involving two molecular weight (MW) populations, using MW of the hydroxyquinoline (305.5 for CQ, 271.2 for PBT2) as a fixed parameter. This experiment was repeated twice.

Size exclusion chromatography (SEC). SEC was conducted using an Akta basic FPLC system and a 10 × 300 mm Superdex S75 size exclusion column (GE Healthcare). Samples containing 15 μM Aβ alone, 15 μM PBT2/CQ alone, or mixtures of Aβ and compound were loaded in 1 ml of PBS supplemented with 0.05 mM EDTA. The column was developed at a flow rate of 1 ml per minute using 1× PBS, pH 7.4, 0.05 mM EDTA, and the chromatogram was acquired using a flow absorbance detector set at 280 nm. The column was calibrated using the low MW calibration kit from GE Healthcare containing aprotinin (MW 6.5 kDa), ribonuclease A (MW 13.7 kDa), carbonic anhydrase (MW 29 kDA), ovalbumin (MW 43 kDa), conalbumin (MW 75 kDa), and blue dextran (MW > 2000 kDa).

To measure the stability of the high MW species present in the absence of hydroxyquinolines and the Aβ-dimeric species induced by the presence of 8-HQs, corresponding fractions were collected and reapplied to the SEC column after intervals of 1 and 2 h.

Small angle x-ray scattering (SAXS). SAXS measurements were acquired at the SAXS/WAXS beamline of the Australian Synchrotron (Kirby et al., 2013). Solutions of Aβ1–42 (1 mg/ml, 221 μM, in PBS) in the presence and absence of 15 μM 8-HQ were analyzed at a camera length of 3.3 m corresponding to a range of momentum transfer $0.005 \leq q \leq 0.35$ Å^{-1} (where $q = 4\pi\sin\theta/\lambda$, 2θ is the scattering angle, and λ is the x-ray wavelength: 1.03 Å at 12 KeV), using a Pilatus 1M detector (Dectris). Data were normalized using an integrated beamstop and intensities put on an absolute scale using distilled water as a standard. To limit radiation damage, 10 frames of 1 s exposure were collected as 50 μl samples/buffers were flowed through a 1.5 mm quartz capillary. The individual frames were compared for agreement before being averaged with the scatterBrain IDL program (http://www.synchrotron.org.au/).

SAXS data were analyzed using the ATSAS software suite (Petoukhov et al., 2007; Petoukhov et al., 2012), including the packages Primus (Konarev et al., 2003) and GNOM, and *ab initio* models generated using Dammif (Franke and Svergun, 2009). Ensemble optimization modeling was conducted using ensemble optimization method (Bernadó et al., 2007) specifying a dimer of Aβ1–42 for the ensemble generation.

Slot blot retention assay. A slot blot apparatus (Bio-Rad) was used as per the manufacturer's instructions. A nitrocellulose membrane (0.22 μm) wetted with PBS was used as a filter. Aβ1–42 at a concentration of 5 μM in 100 μl of PBS was mixed with CQ ranging in concentration from 0 to 25 μM and applied to the slot blot apparatus. Each slot blot well was washed thrice with PBS, and then the apparatus was dismantled and the membrane dried at room temperature. The retention assay was performed in triplicate for each sample, and a total of three replicate assays were conducted. The membranes were then imaged using laser ablation (LA)-ICPMS (detailed methods below) or the individual bands of retained material were excised and eluted off of the membrane using 1% nitric acid. The resulting solution was analyzed by bulk ICPMS (detailed methods below). The ability of PBT2 to compete for the CQ binding site was assayed by supplementing the Aβ solution with PBT2 at a constant concentration of 10 μM. The affinity of PBT2 was then assayed by supplementing the Aβ solution with CQ at 10 μM and titrating PBT2 from 0 to 50 μM. All measurements were conducted in triplicate.

LA-ICPMS. LA-ICPMS analysis and imaging were performed using a NewWave Research UP213 laser ablation unit (Kennelec Scientific), emitting a 213 nm laser pulse in the fifth harmonic. The ablated material was directed to an Agilent 7500ce ICPMS (Mulgrave), fitted with "cs" lenses for enhanced sensitivity. Imaging methods were adapted from those previously described (Austin et al., 2009; Lear et al., 2012). Briefly, a 100 μm laser beam diameter was rastered along the slot blot membrane at 300 μm/s. Iodine (*m/z* = 127) was monitored in time-resolved analysis mode. Images were produced using purpose-designed ISIDAS imaging software (Hare et al., 2010, 2012).

Bulk ICPMS measurements. The elemental content of the retained bands was also analyzed by bulk ICPMS measurements using an Agilent 7700x ICPMS (Mulgrave). For typical instrument parameters, refer to Hare et al. (2013) or Rembach et al. (2014). Briefly, the membrane-containing retained material from the slot blot was carefully excised using surgical scissors and covered with 300 μl of 1% nitric acid. The samples were incubated at room temperature for 2 d, and the solution containing the eluted material was carefully aspirated into 1.5 ml Eppendorf tubes. These samples were introduced the ICPMS using the integrated peristaltic pump sample introduction system. Signals from iodine, copper, zinc, and iron were monitored (*m/z* = 126.9, 63.5, 65.4, and 55.8, respectively).

Binding analysis. The proportion of 8-HQ that is free and the proportion that is bound to Aβ can be determined from either the retention data, as described above, or from the sedimentation velocity data, also as described above. These data can be relatively easily analyzed by Equation 1, where the proportion of bound hydroxyquinoline per Aβ (*R*) is given by the maximal proportion of bound hydroxyquinoline (B$_{max}$), the amount of free hydroxyquinoline (C_f), and the dissociation constant (K_d) as follows:

$$R = \frac{B_{max} \times C_f}{C_f + K_d} \quad (1)$$

This equation was fitted to the titration data using the nonlinear regression tools of Sigmaplot version 12.4, as described previously (Ryan et al., 2011), and converted back to the change in the proportion of sedimenting PBT2 using mass action assumptions.

Analysis of weight average sedimentation coefficient. Analysis of the change in weight average sedimentation coefficient was conducted in a similar fashion to the methods of Schuck (2003). Briefly, the weight average sedimentation coefficient (*Sw*) is proportion to the fractional amount of each species that is present in the sedimenting population. The UV absorbance is arising from the hydroxyquinoline alone; thus, the free Aβ, which has no absorbance at 350 nm, is not affecting the weight average sedimentation coefficient we observe. Assuming that the weight average sedimentation coefficient at the highest concentration of PBT2 is equivalent to that of the complex, we can use simple mass action laws to determine the proportion of complex (AC) and free ligand (C_f). Thereby, we can determine the amount of free Aβ (A_f) and the dissociation constant (K_d). The two pertinent equations (Eqs. 2 and 3) are as follows:

$$S\bar{w} = fAC * SAC \quad (2)$$

where *fAC* is the mol fraction of the Aβ/PBT2 complex and *SAC* is the sedimentation coefficient of the Aβ/PBT2 complex (1.25 S). This equation can be used in conjunction with Equation 3, as follows:

$$Kd = \frac{[AC]}{|A_f| \times |C_f|} \quad (3)$$

to determine the dissociation constant for the complex, as described previously (Schuck, 2003; Bailey et al., 2009; Mok et al., 2011).

NMR analysis. NMR spectra were acquired at 25°C on a Bruker-BioSpin Avance 700 MHz spectrometer equipped with a cryogenically cooled triple-resonance pulsed field gradient probe. Spectra were obtained on samples that were typically 215 μM Aβ1–42 in 150 mM NaCl, PBS at pH 7.0 in ^{1}H$_2$O:^{2}H$_2$O (95:5). Spectra were referenced to 4,4-dimethyl-4-silapentane-1-sulfonic acid at 0 ppm and processed with TopSpin (Bruker-BioSpin).

Multielectrode array (MEA) measurements of Aβ1–42 toxicity. For all MEA experiments, we used an MEA2100 system (MultiChannel Systems), with ground plate heating set at 37°C and 60MEA200/30iR-Ti chips (electrode grid: 8 × 8, 60 TiN electrodes; electrode spacing: 200 μM; electrode diameter: 30 μM; MultiChannel Systems). Dissociated primary mouse cortical neurons (E14) were plated (200,000 cells per chip) and grown on poly-L-lysine-coated (1 mg/ml, prepared in borate buffer) MEA chips using standard culture procedures for 2.5 weeks before experimentation. During this time, the cultures were kept in a humidified atmosphere (95% air, 5% CO_2, 37°C), where they formed stable neuronal networks. Cells were removed from the incubator and baseline levels of activity recorded for each individual experiment (3 min; using MultiChannel Systems MC Rack version 4.5.13 software). Cells were then replaced in the incubator for ~30 min before being removed and treated with either Aβ alone (3 μM final concentration on the chip, n = 6), or in combination with CQ (10 μM final concentration on the chip, n = 4). Vehicle controls were performed separately (n = 2) and had no significant effect on activity. Cells were then returned to the incubator for 24 h before a repeated measurement of levels of activity (3 min). For each individual experiment, the number of spikes and bursts were recorded and values post-Aβ and post-Aβ + CQ normalized to the baseline activity for each experiment. Data were then analyzed with GraphPad Prism 6 for Mac OS X (version 6.0b).
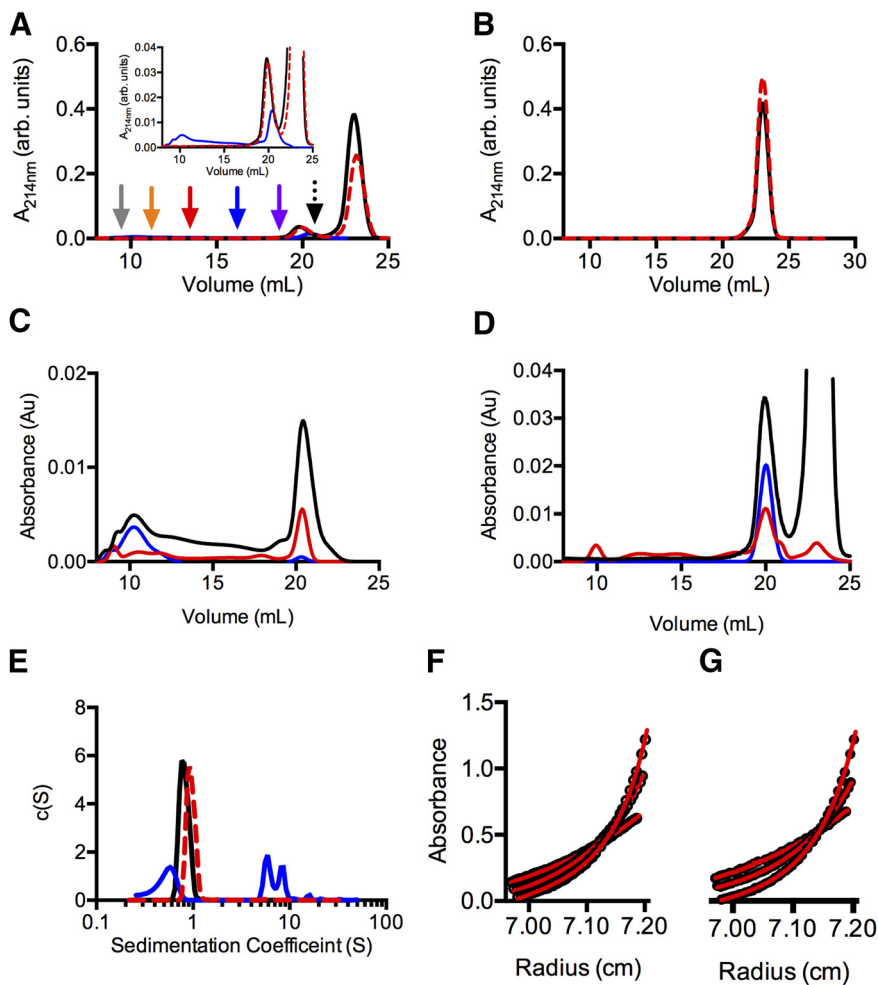
Preparation of soluble fraction C. elegans *homogenate.* C. elegans strains GMC101, dvIs100 [pCL354(unc-54. DA-Aβ1–42) + pCL26(mtl-2:GFP)], and CL2122; dvIs15(mtl-2:GFP) were cultured on 8P media at 20°C as previously reported (McColl et al., 2012). Embryos were developmentally synchronized via alkaline hypochlorite treatment of gravid adults and overnight hatching of L1 larva in S-basal, 0.1 M NaCl and 0.05 M K_xPO_3 buffer, pH 6.0 (Brenner, 1974). Approximately 50,000 L1 larvae were transferred to 8P media for 24 h and then an additional 24 h on 8P media ± PBT2 or CQ, with DMSO as the vehicle (final concentration 0.5% v/v). Populations were shifted to 25°C for 24 h to allow the Aβ-induced paralysis phenotype to manifest (McColl et al., 2012). Samples were washed from media with S-basal, and eggs, larvae, and debris were removed via filtration through 40 μm nylon filters (BD Sciences). Approximately 0.5 ml (wet pellet) of adults per replicate was frozen in liquid N_2 for lysis. Samples were disrupted in chilled PBS (Invitrogen), with an ice-chilled bath sonicator (Bioruptor, Diagenode), using 5 on– off cycles of 30 s durations on high power (320 W), then clarified by ultracentrifugation (100,000 × g for 30 min at 4°C). Supernatant was removed and kept on ice or immediately used.

Aβ oligomer ELISA assay. Aβ oligomer levels were determined using the sandwich ELISA with the same antibody used for both capture and detection. The procedures and buffers are similar to those described previously for the monomeric Aβ ELISA (White et al., 2006; Lim et al., 2011). The assay was conducted in 384 well, high-binding polystyrene plates (Greiner). The plate was precoated with 25 μl of 10 μg/ml W02 monoclonal antibody (epitope Aβ5–8) (Ida et al., 1996) in 50 mM sodium carbonate, pH 9.6, at 4°C overnight. After washing with PBST (PBS containing 0.05% Tween), the plate was blocked with 0.5% (w/v) casein in PBS buffer, pH 7.4, to minimize nonspecific binding, and washed with PBS before addition of samples and WO2-biotin (final concentration 0.3 μg/ml, made from a 1 mg/ml stock) and incubated overnight at 4°C. The

Figure 1. The effect of CQ and PBT2 on Aβ1–42 aggregation. **A**, Aggregation of 5 μM Aβ1–42 was monitored by ThT fluorescence in the absence (blue) and presence of 10 μM CQ (black) or PBT2 (red). Inset, **I**, Structure of PBT2. **II**, Structure of CQ. **B**, Titration of the effective concentration for inhibition of ThT signal for CQ (black) and PBT2 (red) Aβ1–42 alone is also plotted, showing no significant change over the time frame (blue). **C, D, E**, Representative images of the grids for Aβ1–42 alone (**C**) and in the presence of CQ (**D**) and PBT2 (**E**). Images are representative ~20 images acquired over the EM grids. **F**, The effect of 10 μM PBT2 (red) and CQ (black) on the ThT signal of preformed fibrils (blue represents 5 μM monomer equivalent, alone; t = 0; open bars) after 5 min of incubation (average of 3 measurements). **G**, The effect of 10 μM PBT2 (red) and CQ (black) on the ThT signal of preformed fibrils (blue represents 5 μM monomer equivalent, alone) over time (average of 3 measurements). **H, I**, The proportion of protein in the supernatant and pellet fractions of freshly refolded (**H**) or fibrillar Aβ (**I**) incubated alone (blue) and in the presence of CQ (black) or PBT2 (red) for 24 h.

Figure 2. The effect of hydroxyquinolines on Aβ1–42 self-association. **A**, The distribution of Aβ1–42 species present in samples of Aβ1–42 alone (10 μM; blue line) or Aβ1–42 (10 μM) mixed with CQ (10 μM; black line) or PBT2 (10 μM; red line) was analyzed by SEC using a 10 × 300 Superdex 75 column (flow rate 0.75 ml/min, equilibrated in PBS). Inset, Full-scale plot. Arrows indicate the migration of MW standards. Purple arrow indicates ribonuclease A (MW 13.7 kDa). Blue arrow indicates carbonic anhydrase (MW 29 kDA). Red arrow indicates ovalbumin (MW 43 kDa). Orange arrow indicates conalbumin (MW 75 kDa). Gray arrow indicates blue dextran (MW > 2000 kDa). Black arrow indicates the migration of Aβ1–42 monomer. **B**, Same as for **A**, except that the samples are PBT2 (10 μM; red line) and CQ (10 μM; black line) alone. **C**, **D**, The stability of oligomers was investigated by fractionating and reapplying the high MW oligomers formed by Aβ1–42 alone (**C**) and the low MW oligomer formed by Aβ1–42 in the presence of 8-HQ (**D**) after 1 h (blue line) and 2 h incubation (red line). The original trace for both samples from **A** is provided for comparison (black line). **E**, The distribution of Aβ1–42 species present in samples of Aβ1–42 alone (10 μM; blue line) or Aβ1–42 (10 μM) mixed with equimolar CQ (black line) or equimolar PBT2 (red dashed line) was reinvestigated using a sedimentation velocity experiment. **F**, **G**, Sedimentation equilibrium analysis of equimolar Aβ1–42 in the presence of CQ (**F**) or PBT2 (**G**). Analysis of these data gives a MW of ~10 kDa (calculated from fitting to a noninteracting species model in SedPhat12). Solid lines indicate fit. Symbols represent every fourth data point.

collected across the entire elution, and the amount of monomeric Aβ peptide in each fraction was determined by sandwich ELISA, following the protocol for the oligomer ELISA described above, except that the detection antibody was substituted for 1E8-biotin (epitope 17–22), which, as it has a different detection epitope from the capture antibody (WO2), will detect monomeric, oligomeric, and fibrillar Aβ1–42 peptides.

Results

The effect of PBT2 on Aβ self-association

Hydroxyquinoline effects on Aβ1–42 fibril formation were determined using a continuous ThT assay. Measurements, conducted in triplicate and averaged, indicate that Aβ1–42 alone followed a sigmoidal increase in ThT fluorescence intensity over a 20–24 h time period, whereas Aβ in the presence of CQ or PBT2 did not produce a significant increase in ThT fluorescence (Fig. 1A). This was consistent with our previous studies on inhibitory compounds (Ryan et al., 2012). Inhibition was concentration dependent, with an IC$_{50}$ of ~4.7 μM and 5.1 μM for CQ and PBT2, respectively (Fig. 1B). One possibility for this phenomenon is that the hydroxyquinoline competes for ThT-binding sites on Aβ amyloid fibrils. We tested this hypothesis by adding CQ and PBT2 to preformed fibrils simultaneously with an equimolar amount of ThT and monitored the change in ThT fluorescence over time (Fig. 1C,D). Over short time frames (5 min), there was no significant change in ThT fluorescence; however, over longer time frames (24–48 h), there was an ~50% reduction in the fluorescence intensity of the samples containing CQ or PBT2 compared with that of Aβ alone, which was not significantly changed over the course of the experiment. This was suggestive of longer time processes, such as a disturbance of the equilibria associated with fibril formation toward nonfibrillar species, resulting in a slow redistribution of Aβ1–42 from fibrillar to monomeric nonfibrillar species, rather than competition for binding sites, which would be expected to occur over short time frames. Furthermore, electron micrographs of the time course samples from Figure 1A (representative of three separate time course experiments, Fig. 1E–G) show the presence of fibrillar aggregates only in the Aβ1–42 alone samples; in the Aβ/CQ and Aβ/PBT2 cases, there were no aggregates of any type to be observed. These results are strongly indicative that these 8-HQ do not interfere with ThT binding directly, which is consistent with previous results obtained with a radiolabeled form of CQ that showed that ThT does not compete with 8-HQs for fibril binding sites (Opazo et al., 2006). Further evidence for a loss of amyloid, rather than competition with ThT, was provided by a pelleting assay. The level of protein in the pellet fraction was

plate was washed with PBS and europium-labeled streptavidin (final concentration 1 nM, made from a 10 μM stock) added for 1 h at room temperature. After a final wash, the plate was developed with a commercial enhancement solution, which allows the europium to become fluorescent. Time-resolved analysis was performed using a Wallac Victor² 1420 Multilabel Plate Reader (PerkinElmer) with excitation at 340 nm and emission at 613 nm, a delay of 400 μs, and a measurement window of 400 μs. Relative fluorescence levels minus the background were used for each sample as an indication of the Aβ oligomeric levels. Each measurement was performed in triplicate.

Size exclusion analysis of C. elegans homogenates. The supernatant of *C. elegans* homogenate (100 μl) was applied to a 10 × 300 mm Superdex S75 size exclusion column (GE Healthcare) using an Agilent 1200 series HPLC. The column was developed at a flow rate of 1 ml per minute using 1× PBS, pH 7.4, 0.05 mM EDTA, and the chromatogram was acquired using a flow absorbance detector set at 280 nm. Fractions (750 μl) were

reduced ~50% upon treatment with hydroxyquinoline for 24 h, consistent with the changes in the amount of ThT fluorescence (Fig. 1*H*), indicating a loss of aggregated material as well as a loss of cross β structure.

To further investigate the effect of these 8-HQ on Aβ1–42 self-association, we used SEC under native conditions. Freshly resuspended Aβ was confirmed to exist as an equilibrium mixture of large (>30 kDa) and small (<20 kDa) oligomers (Fig. 2*A*; 60% high MW, 40% low MW). Application of 1:1 Aβ/8-HQ mixtures to the column resulted in the elution of two major peaks with retention volumes of ~18.8 and 21 ml, with no evidence of the high MW species. The peak at 21 ml was replicated by conducting the experiment in the presence of PBT2/CQ only (Fig. 2*B*), indicating that this peak represented the free ligand, whereas the peak at 18.8 ml most likely represented a small, low MW Aβ oligomer. Monomeric Aβ1–42 peptides eluted from this column at ~19.5 ml.

By fractionating the elution and reapplying the fractionated sample to the column at various time intervals, we investigated the stability of the major oligomers present in the samples. As the major oligomer for Aβ1–42 was centered at ~10 ml, a 2 ml fraction from 9 to 11 ml was manually collected, and half was reinjected at 1 h, and after 2 h (Fig. 2*C*). Over this time frame, the peak at 10 min slowly disappeared, and the distribution shifted to resemble the original SEC chromatogram of Aβ1–42 alone. This indicated that all of the oligomers in this sample were in a slow equilibrium and that the high MW species dissociated in the absence of low MW species. Similarly, the 8-HQ-stabilized species at 18 ml was collected manually in a 2 ml fraction from 17 to 19 ml and reapplied to the SEC column (Fig. 2*D*). Over this time frame, there was a decrease in the peak at 18 ml, and the appearance of both higher and lower MW peaks, consistent with dissociation of the complex resulting in free CQ and Aβ capable of self-associating into higher MW peaks. This dissociation of the stabilized species indicated that the dimer was not stable in the absence of excess hydroxyquinolines, suggesting a low-affinity interaction.

The effects of the 8-HQ on the aggregation state of Aβ were further explored using analytical ultracentrifugation (Fig. 2*E–G*). Our previous work has shown that low MW Aβ species are formed upon addition of small amphipathic detergent molecules to freshly prepared Aβ, which is itself a heterogeneous mix of small and large oligomers (Ryan et al., 2012). As PBT2 and CQ absorb strongly in the UV range and could potentially bias the
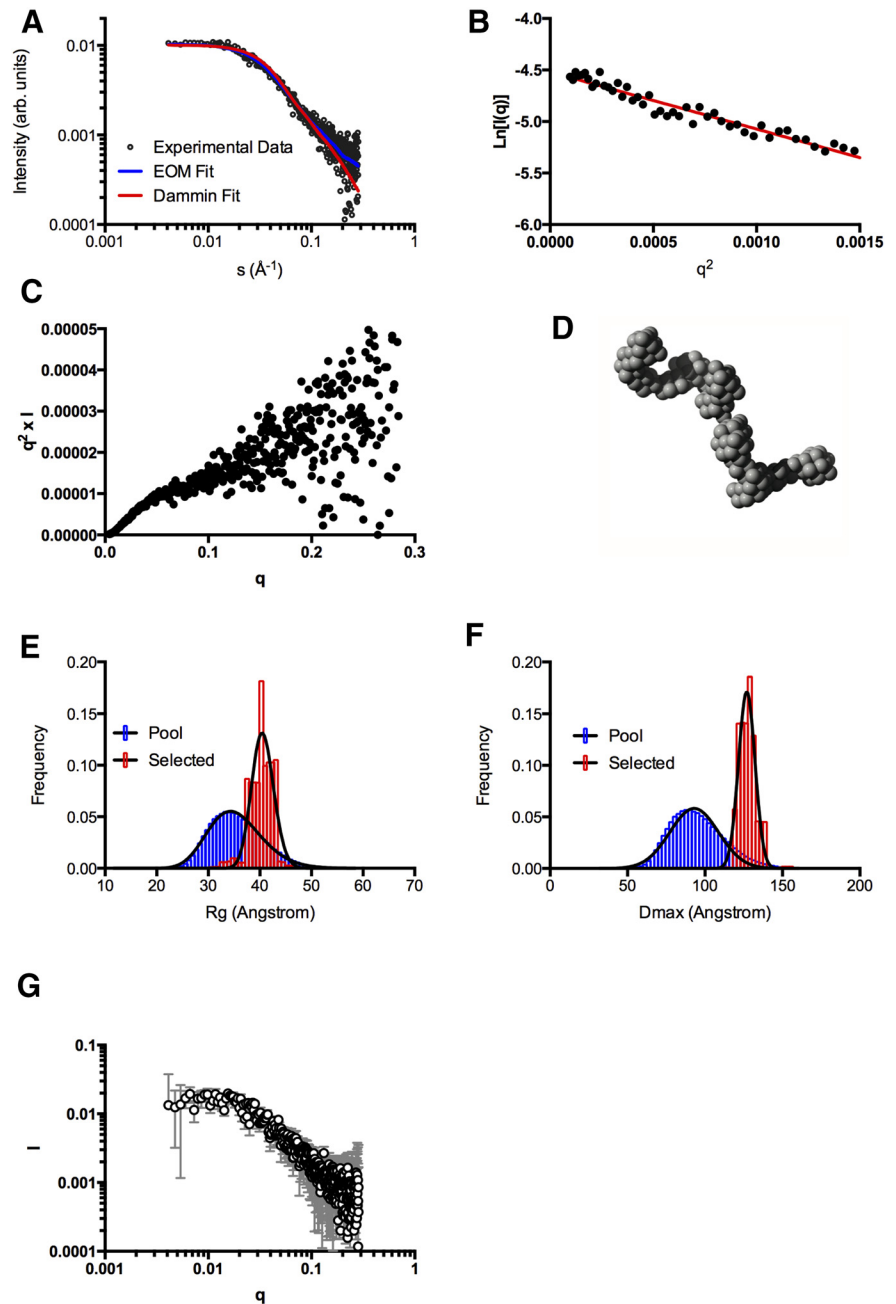
Figure 3. SAXS analysis of the Aβ/CQ complex. *A*, SAXS data for Aβ1–42 (0.2 mg/ml, ~20 μM) in the presence of 20 μM CQ was acquired at the Australian synchrotron. *B*, Guinier analysis of the CQ data in *A*. *C*, Kratky analysis of the CQ data in *A*. *D*, De novo reconstruction of the scattering entity induced by CQ using Dammif. Line indicates overall dimension (D_max). *E*, *F*, Ensemble optimization modeling of the CQ-induced Aβ1–42 dimers provides information on the distribution in the radius of gyration (Rg, *E*) and maximal dimension (D_max, *F*) in relation to a pool of randomly generated structures: blue represents pool; red represents selected structure parameters. *G*, SAXS data for Aβ1–42 (0.2 mg/ml, ~20 μM) in the presence of 20 μM PBT2 (red squares) were also acquired at the Australian synchrotron but had too high a ratio of signal-to-noise and thus were not of sufficient quality for further analysis.

analysis, we monitored the oligomeric status of Aβ in solution using trace amounts of fluorescently labeled Aβ peptide. Aβ alone, as has previously been observed (Ryan et al., 2012), displays a main (~60% of the total) peak at 0.6 S (MW ~5 kDa) and a distribution of populations with sedimentation coefficients ranging from 5 to 50 S (Fig. 2*E*; MW ~21–1000 kDa). Addition of PBT2 or CQ suppressed the formation of large aggregates (sedimentation coefficients 5–50 S) and shifted the low S peak from 0.6 S to 1.2 S (approximate MW of 10–15 kDa) (Fig. 2*E*). Sedi-
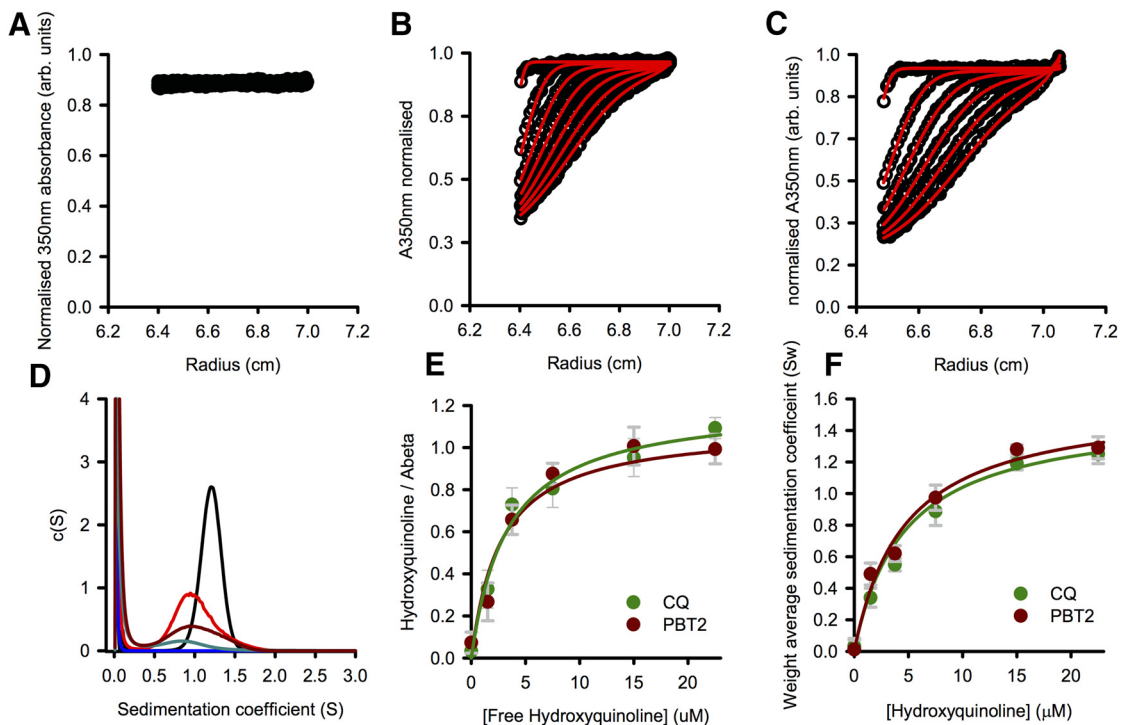
Figure 4. Investigation of the association of PBT2 and CQ with Aβ1–42. **A–C**, Sedimentation velocity profiles acquired using 350 nm absorbance for PBT2 alone, PBT2 + 0.5 equivalents of Aβ, and PBT2 + 1.5 equivalents of Aβ1–42, respectively. Data are normalized to provide better representation of the proportion of sedimenting material. **D**, c(S) distributions for PBT2 in the absence or in the presence of increasing proportions of Aβ (15 μM PBT2, 15 μM Aβ, black line; 7.5 μM PBT2, 15 μM Aβ, red line; 5 μM PBT2, 15 μM Aβ, orange line; 2.5 μM PBT2, 15 μM Aβ, green line; 0.1 μM PBT2, 15 μM Aβ, blue line). **E**, Proportion of sedimenting optical density as a function of CQ (dark green symbols) or PBT2 (dark red symbols) concentration. **F**, Weight average sedimentation coefficient plotted as a function of CQ (dark green symbols) or PBT2 (dark red symbols) concentration. **E, F**, Lines through the data indicate fits of the equations described in the text and indicate a K_d of ∼1–10 μM.

mentation velocity measurements are affected by molecular geometry so a sedimentation equilibrium experiment was conducted to accurately determine the mass of the species. Aβ in the presence of PBT2 (Fig. 2F) or CQ (Fig. 2G) was determined to have a molecular mass of 10.2 ± 0.3 kDa and 9.95 ± 0.26 kDa, respectively. It is not possible to accurately assess the mass of Aβ alone using this method, as equilibrium between sedimentation and diffusion is never reached, presumably because of an equilibrium distribution between aggregated and nonaggregated forms of Aβ that changes over time.

The above results indicate that the presence of equimolar or greater hydroxyquinolines induces the formation of a relatively stable population of low MW species of Aβ. We chose to investigate these species further using Synchrotron SAXS. Aβ in the presence of CQ provided high-quality data for analysis (Fig. 3A), but Aβ in the presence of PBT2 did not provide data of sufficient quality (Fig. 3G) and, thus, was not used in this analysis. Guinier analysis of the CQ:Aβ SAXS data demonstrates that the complex was clearly oligomeric, with an average radius of gyration (R_g) of 35.6 Å (Fig. 3B) [expected R_g for unfolded monomeric Aβ1–42 based on sequence is 18.3 Å (Kohn et al., 2004)], and a Kratky plot representation of the data is consistent with that expected for partially unfolded Aβ (Fig. 3C). The MW of the CQ:Aβ complex estimated from the forward scattering intensity (I_0 = 0.010) was ∼11–12 kDa, consistent with the results from analytical ultracentrifugation (AUC) and SEC. The particle distance distribution function, $P(r)$, was calculated via indirect Fourier transformation of the scattering data with Gnom (Svergun, 1992) giving a maximum diameter (D_{max}) of 122.45 Å and an average real space R_g of 37.8 Å. *De novo* reconstruction of the shape of the CQ/Aβ com-

plex was performed using the bead modeling program Dammif (Franke et al., 2009), yielding extended structures with dimensions consistent with dimeric Aβ (Fig. 3D). The orientation of the Aβ1–42 molecules in the dimer cannot be determined by SAXS analysis because of the nonsequence dependence of x-ray scattering.

As the Kratky plot representation and the significantly extended *ab initio* model suggest a flexible system, an ensemble approach to modeling was subsequently conducted using the ensemble optimization method (Bernadó et al., 2007). This approach generates a pool of conformations (typically 10,000 structures) based on the input protein sequence, and specified oligomerization state (in this case a dimer), and then uses a genetic algorithm to select a subset of structures that best fit the experimental SAXS data. This analysis provides distance distributions (R_g and D_{max}) that describe the predominant structural features of the sample in solution. These distributions are shown in Figure 3E, F, where the distributions for the selected structures that fit the SAXS data (fit shown in Fig. 3A, red line) provide relatively narrow distributions relative to the initial pool, with modal values of 34.5 Å (R_g) and 128.6 Å (D_{max}). These values are larger than the modal value for the pool distribution indicating that the CQ/Aβ complex is not simply a distribution of random coil dimeric structures, but a more specific extended dimeric structure, and the narrow R_g/D_{max} distributions also suggest that the complex is at least partially folded.

Analysis of the interaction of 8-HQ with Aβ
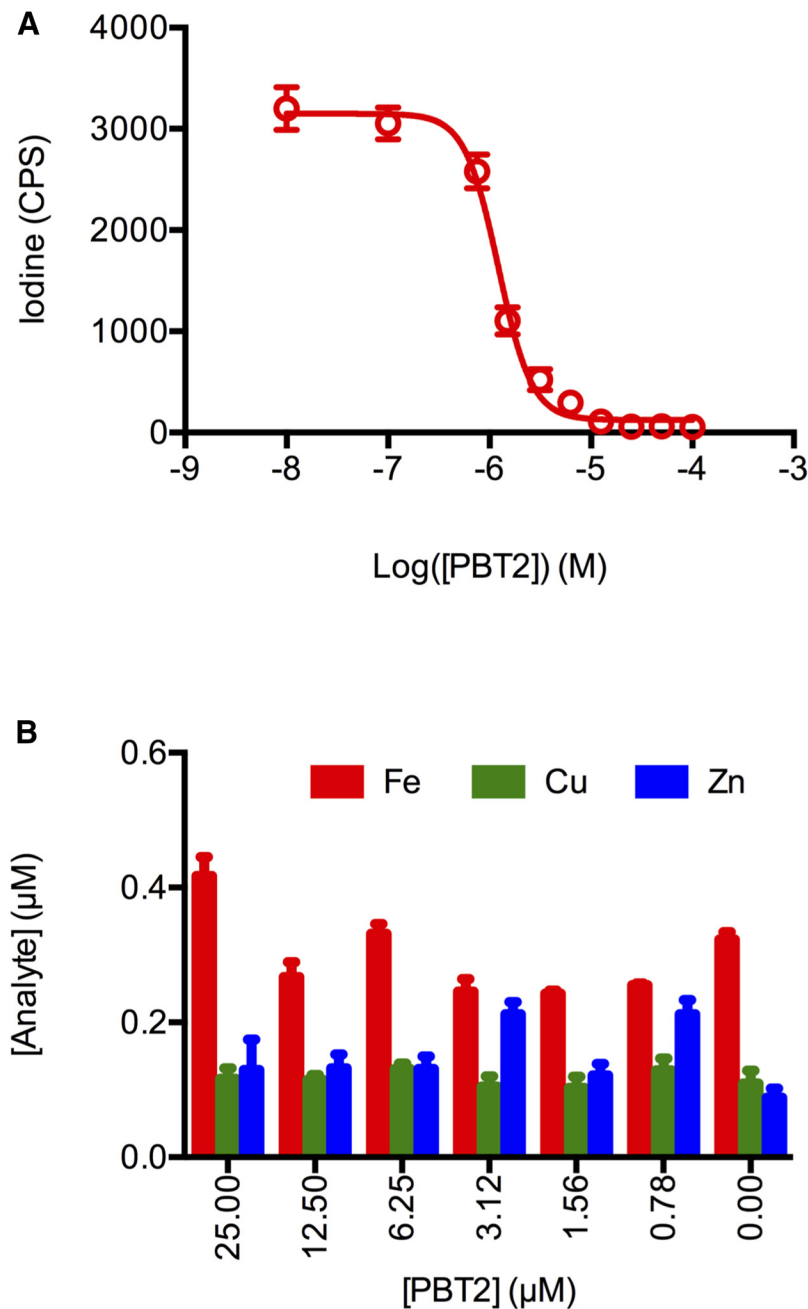The ThT, pelleting, AUC, SEC, and SAXS results in combination indicate that Aβ in the presence of hydroxyquinoline is most
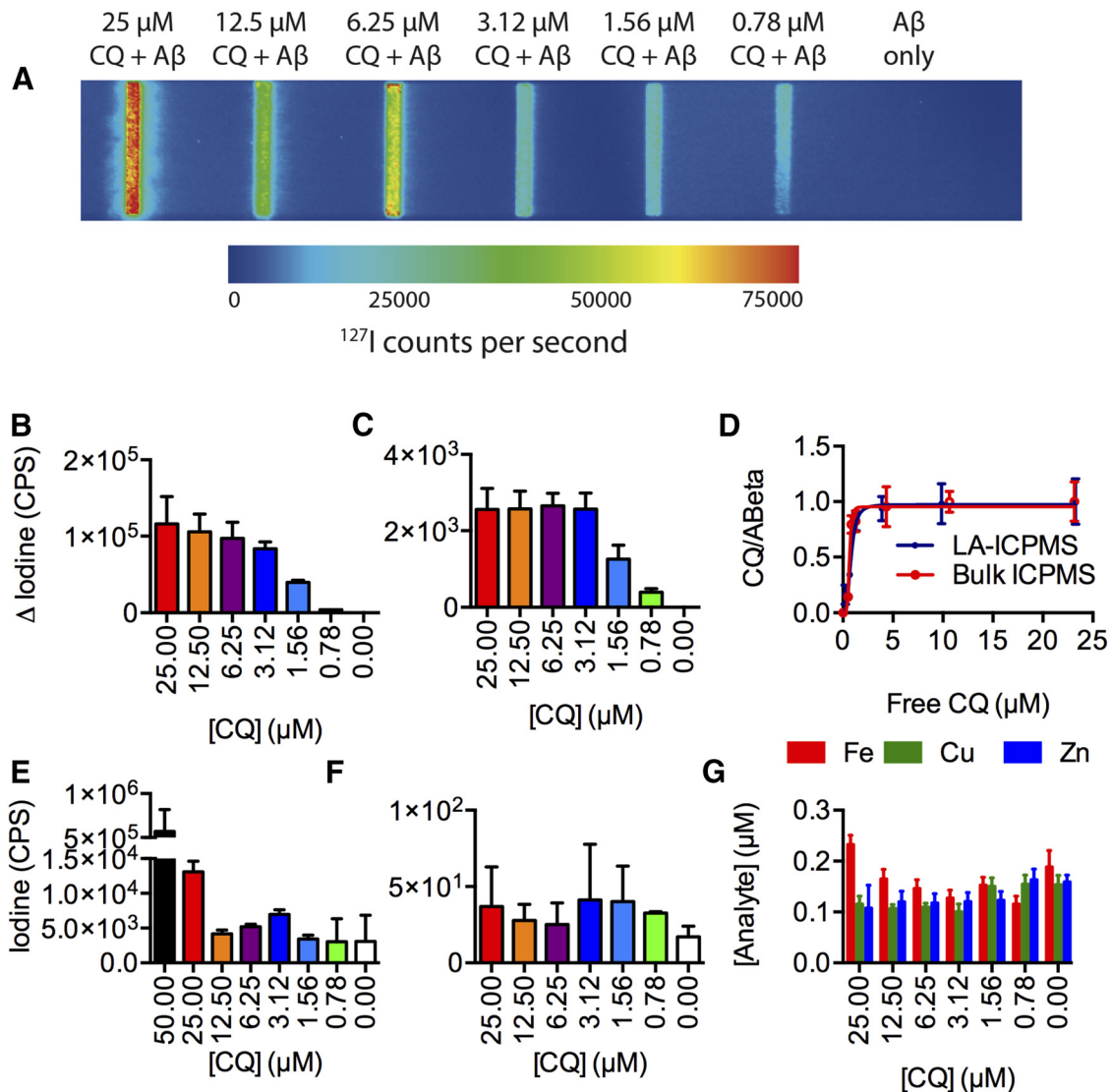
Figure 5. Elemental analysis of the CQ interaction with Aβ1– 42. **A**, LA-ICPMS detection of iodine was used to generate an image of a slot blot assay where Aβ1– 42 was mixed with increasing concentrations of CQ (as marked). Retained iodine is an integral part of CQ and is quantitative of the amount bound to Aβ. **B**, The concentration dependence of iodine retention in the slot blot assay obtained through quantitation of the image in **A**, corrected for signal from CQ only samples. **C**, Quantitation of retained iodine, obtained through excision of bands on the nitrocellulose and extraction using nitric acid and measurement using standard bulk ICPMS analysis. **D**, The retained CQ, determined by each method (red represents bulk ICPMS analysis; blue represents laser ablation ICPMS analysis), was converted to proportion CQ bound per Aβ, which was then plotted as a function of free CQ. This was analyzed to obtain a K_d of ∼1 μM. **E**, Retained CQ as a function of concentration in the absence of Aβ, LA-ICMPS. **F**, Retained CQ as a function of concentration in the absence of Aβ, bulk ICMPS. **G**, Quantitation of retained iron, copper, and zinc, using the excision and extraction ICPMS method.

likely a low MW complex, of approximately two 8-HQ (∼700 Da) and two Aβ molecules (9024 Da), giving a stoichiometry of 1 hydroxyquinoline:Aβ molecule. These data, however, do not indicate the affinity of Aβ for 8-HQ. To address this, we initially took advantage of inherent UV absorbance of the 8-HQ molecules, which provide an excellent tool to monitor the association of these compounds with Aβ. Analyzing the absorbance unique to a species in solution, such as PBT2 or CQ, is a powerful tool to measure direct interactions, as exemplified by studies investigating the interaction of 7-nitrobenz-2-oxa-1,3-diazol-4-yl amino-labeled phospholipids with apoC-II (Mok et al., 2011; Ryan et al., 2011), or the interaction of Alexa-488 labeled DNA with Klenow fragment (Bailey et al., 2009). PBT2 and CQ are particularly suited to this approach because they have a low molecular mass and do not sediment effectively in the aqueous-based buffer systems of the experiment. Figure 4 shows the absorbance of 15 μM

PBT2 as a function of radial position in the absence of Aβ (Fig. 4A), and PBT2 at 7.5 μM (Fig. 4B) and 22.5 μM in the presence of 15 μM Aβ (Fig. 4C). The addition of Aβ induces the formation of boundaries in the absorbance data, which are dependent on the concentration of PBT2. Similar data for CQ were also acquired and showed a similar trend. This indicates that there is a specific saturable interaction between these two molecules. From the absorbance of PBT2 (or CQ), we can estimate the amount of hydroxyquinoline required to saturate the sedimentation analysis (∼15 μM), which gives a stoichiometry of 1:1 (Fig. 4D). Further analysis of the data at the saturating concentration with the c(S) model in SEDFIT9.4 showed that PBT2 and CQ were associated with an Aβ species having a sedimentation coefficient of 1.25 ± 0.1 S (∼11–14 kDa) (Fig. 4E). Thus, the observed complex has an approximate MW of 10 kDa and consists of two Aβ peptides and two hydroxyquinoline molecules, giving a 2:2, or apparent 1:1,

Figure 6. Elemental analysis of the PBT2 interaction with Aβ1–42. **A**, Titration of PBT2 against a set concentration of CQ (10 μM) in the presence of Aβ1–42 (10 μM) resulted in a loss of iodine signal. Analysis of these data indicates a K_d of 1.1 μM for the interaction of PBT2 and Aβ. **B**, Quantitation of retained iron, copper, and zinc, measured using the bulk ICPMS method.

of the methods used and in the presence of an excess of EDTA. Under these conditions, the formation of such a metal ion ternary complex is unlikely; however, categorical, conclusive evidence for the absence of metal ion involvement in the interaction is difficult to address using these assays. Thus, we used ICPMS to determine whether the Aβ/hydroxyquinoline was a ternary complex involving metal ion or a metal independent binary interaction. ICPMS analysis also provides detection that is significantly more sensitive and specific for the compound than the other methods we have used. The approach involved a slot blot membrane retention assay, similar to those used for radioisotope measurements of protein-CQ interactions (Opazo et al., 2006), where the protein (Aβ peptide) is mixed with an increasing concentration of ligand (CQ) and is applied to a nitrocellulose membrane. Instead of using radiation counting to detect the proportion of bound ligand, we used ICPMS to measure the presence of various elements, including iodine (as the unique heteroatom component of CQ), copper, zinc, and iron. For confirmation of our results, we did this analysis via two different sample introduction methods, in two separate locations. First, we used LA-ICPMS to directly measure the elements retained on the nitrocellulose membrane, providing the image in Figure 5A. Second, we used a digestion protocol to solubilize the retained elements, and introduced this solubilized material into the ICPMS with standard liquid handling approaches (solution nebulization ICPMS). The image in Figure 5A shows a clear trend where increasing the concentration of CQ in the Aβ/CQ mixture results in increased retention of iodine, consistent with the formation of a CQ/Aβ complex. This is quantified for LA-ICPMS in Figure 5B, and for bulk ICPMS in Figure 5C, corrected for retention of CQ alone by subtraction of the values shown in Figure 5E, F. Metal ions, including iron, copper, and zinc, showed no significant retention (Fig. 5D). As this is a retention assay and we did not observe any metal present in our hydroxyquinoline, Aβ, or buffer reagents, this indicates that there is no metal retained with the complex. Thus, these metal ions are not significantly associated with the Aβ/CQ complex and, under the conditions used in this study, there is no evidence for the formation of a ternary complex between Aβ, CQ, and a metal ion. Retention of CQ in the absence of Aβ was not significant at the concentrations where CQ is soluble; however, at 50 μM, where CQ is insoluble, we observed appreciable iodine signal (shown in Fig. 5E).

The retained iodine signal is directly proportional to the concentration of the Aβ/CQ complex and consequently provides a

stoichiometry. Analysis of the concentration titration data for both the proportion of sedimenting PBT2 and CQ, and the weight average sedimentation coefficient (obtained by integrating the c(S) distributions, representative data for PBT2 shown in Fig. 4D), indicated an apparent dissociation constant in the low micromolar range (Fig. 4E and Fig. 4F, respectively), which is a relatively weak interaction that appears to have a very significant effect on the self-association of Aβ.

There is a body of research using cell culture and electron paramagetic resonance spectroscopy that suggests Aβ is capable of forming a metal ion-mediated ternary complex with PBT2/CQ (Kenche et al., 2013). The AUC and SEC results were performed with buffers where the metal content is below the detection limit

measure of the free CQ. These data can be plotted to produce a classical binding curve (Fig. 5D). Nonlinear regression, with a single site binding model, of these data provides a stoichiometry of 1 CQ:1 Aβ and a dissociation constant (K_d) of ~1 μM ($R^2 = 0.95$ for LA-ICPMS, 0.91 for solution nebulization ICPMS).

Relative affinity of PBT2 and CQ for Aβ

As PBT2 does not contain iodine, we cannot use the above retention assay to directly interrogate the affinity of PBT2 for Aβ. However, we can use competition between the CQ and PBT2 to determine the relative affinity of these compounds for Aβ. Titration of PBT2 against a set concentration of 10 μM CQ in the presence of Aβ resulted in a concentration-dependent decrease in the retained iodine signal, consistent with a classic "cold" competition assay (Fig. 6A). Analysis of the data with a standard one-site competitive binding model provided an approximate equilibrium inhibitor dissociation constant (K_i) of 1.1 μM for the interaction of PBT2 to Aβ. Consistent with the CQ results, there was also no change in the status of any of the metal ions upon titration of PBT2 (Fig. 6B).

Molecular analysis of the Aβ/PBT2 interaction

The observation of apparent hydroxyquinoline:Aβ1–42 complexes with AUC, SEC, and SAXS and an apparent dissociation constant of <10 μM led us to attempt nuclear magnetic resonance analysis of the samples. Using natural isotopic abundance in the peptide sample, concentrations of 1–2 mg/ml (214–428 μM) were required for sufficient sensitivity, and this precludes the use of CQ in these experiments, as its solubility is ~30 μM in our buffers. PBT2 has no such constraint; thus, these experiments were conducted solely with this 8-HQ. The majority of the Aβ1–42 resonances are unperturbed in the presence of the drug PBT2 (Fig. 7). In the presence of one equivalent of PBT2 to Aβ1–42, resonances associated with PBT2 are significantly broadened with a small chemical shift perturbation (0.04 ppm for the methyl resonances) from the positions of PBT2 in the absence of Aβ and reflect a very low affinity interaction that is in intermediate exchange on the NMR time scale under these conditions (Fig. 7).

Cellular toxicity of the hydroxyquinoline stabilized Aβ1–42 oligomer

To investigate the effect of these Aβ/hydroxyquinoline complexes on neuronal function and toxicity, we conducted an MEA experiment (Fig. 8). This provides information on the effect of a compound or peptide on a neuronal network. We specifically investigated the spikes (Fig. 8A) and bursts (Fig. 8B) of activity in cultured mouse primary cortical neurons after treatment with Aβ
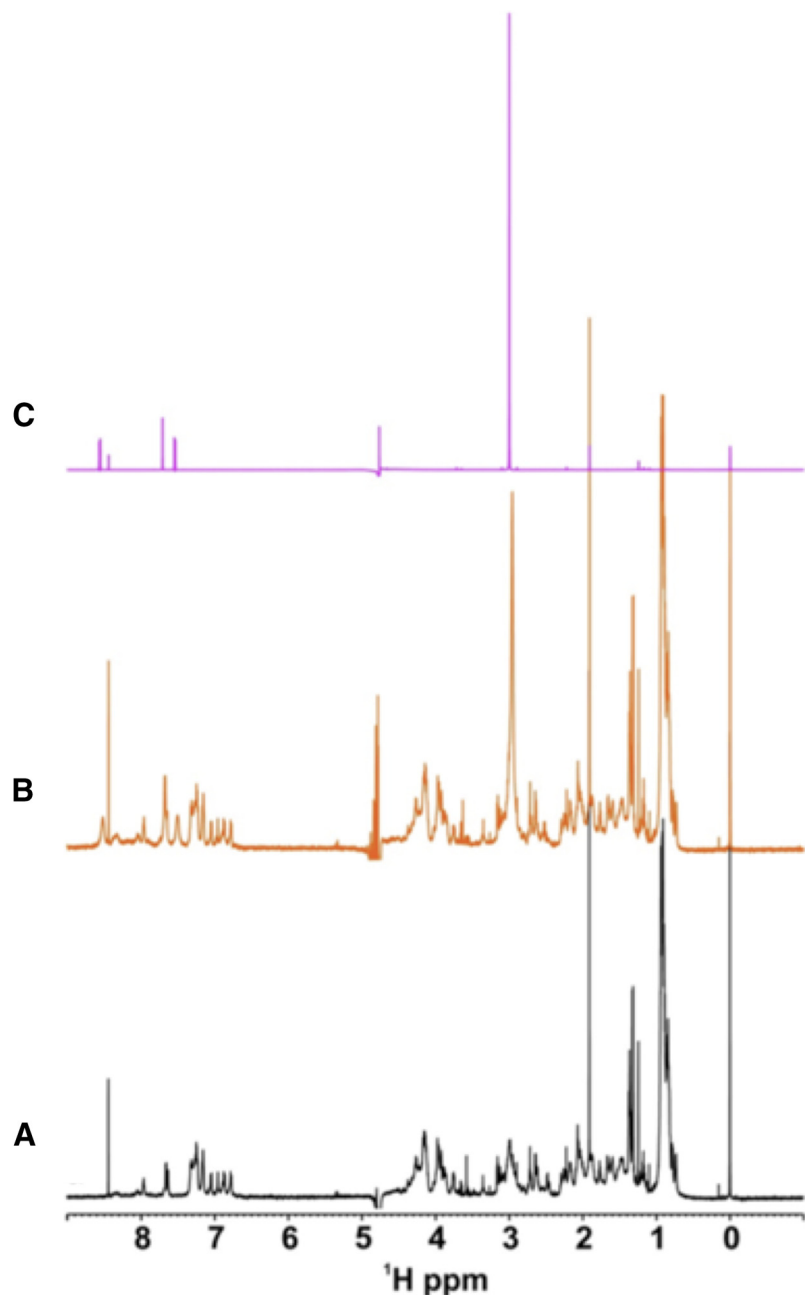
Figure 7. 1D ^{1}H NMR spectra of Aβ1–42 in the presence and in the absence of PBT2. **A**, PBT2 alone. **B**, Aβ1–42 with 1 equivalent PBT2. **C**, Aβ1–42 alone. Spectra were acquired at 700 MHz in 150 mM PBS, pH 7.0, and 25°C.

alone or Aβ mixed with approximately twofold concentrations of CQ. Aβ alone significantly decreased the activity of the neuronal culture, consistent with previous measures of Aβ toxicity to neuronal cultures. Interestingly, addition of Aβ and CQ not only stopped the reduction in activity but also resulted in a significant increase in activity, consistent with the stabilized Aβ dimer being nontoxic, and CQ enhancing the activity of neurons.

In vivo effects of PBT2 on Aβ1–42 oligomerization in C. elegans

In cell culture, we have shown that the stabilized complex is nontoxic. To investigate the effect of 8-HQs in whole animal models of Aβ toxicity, we used a transgenic C. elegans model that displays paralysis upon expression of Aβ1–42. We previously reported that PBT2 can reduce the toxicity of Aβ1–42 in transgenic C.

A

B
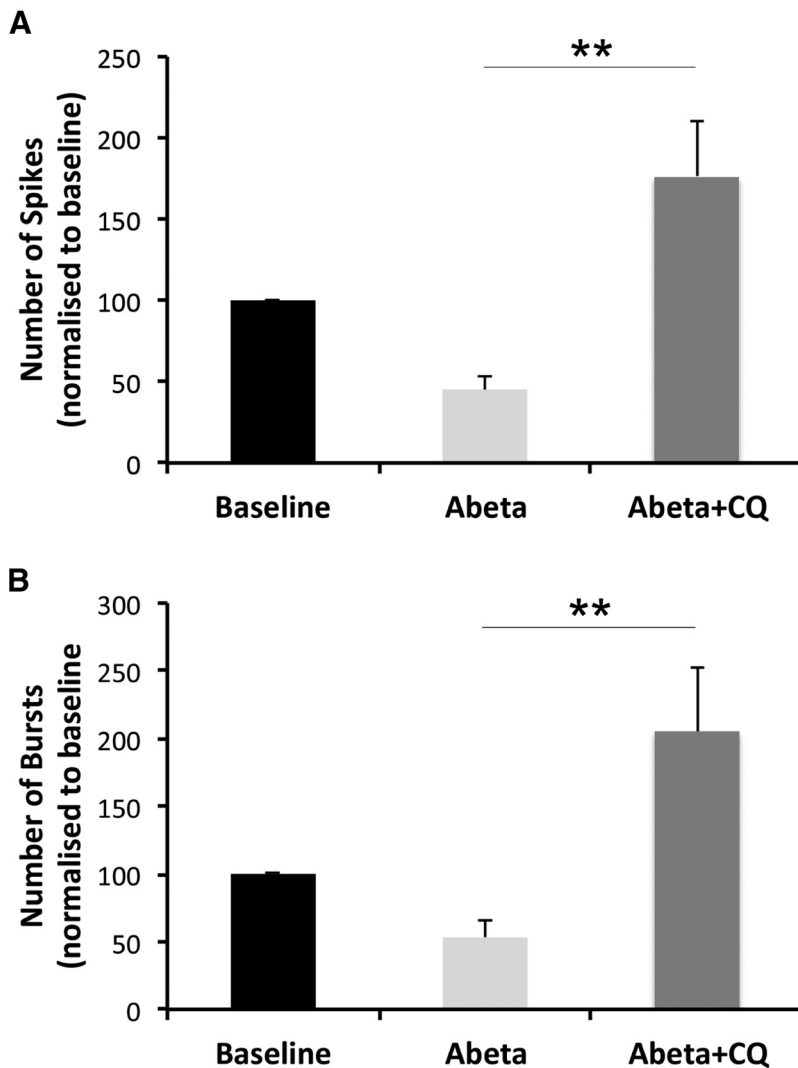
Figure 8. Assessment of the toxicity of CQ-induced Aβ dimers by multielectrode array analysis. Recording of neuronal activity in primary mouse neuronal cells treated with either Aβ or Aβ + CQ. *A*, The total spike activity, normalized to baseline recordings (set to 100%). *B*, The total number of bursts, normalized to baseline recordings (set to 100%). **$p < 0.01$.

gomerization state upon treatment, this assay is not quantitative, nor does it provide any indication of the molecular mass of the oligomeric species. Thus, we also examined soluble extracts of *C. elegans* transgenics using size exclusion fractionation on the Superdex 75 column (Fig. 9C). This analysis shows a clear and significant decrease in high MW Aβ and a small increase in low MW Aβ species (quantified by measuring the area under each respective peak; Fig. 9D), consistent with the AUC and SEC observations described above. Interestingly, the biologically derived Aβ oligomers appear larger than the synthetically derived species. This may be due to increased time to aggregate, a variety of post-translational modifications, or any number of macromolecular interactions that may occur in the complex biological milieu of a whole animal model. Importantly, although treatment with 8-HQ altered the levels of soluble Aβ oligomers *in vivo* as predicted from the *in vitro* studies, the treatment did not completely abolish the presence of Aβ oligomers in *C. elegans*. This result is consistent with both partially reduced phenotype rather than complete prevention of Aβ-induced toxicity (McColl et al., 2012) and with the idea of 8-HQ having multiple modes of action.

Discussion

We have investigated the 8-HQ (CQ) and the novel 8-HQ compound PBT2 for activity in modulating Aβ1–42 self-association and aggregation through a direct interaction. Our aggregation assay results show that these compounds are capable of inhibiting amyloid fibril formation (Fig. 1), and the AUC, SEC, and SAXS results show that both PBT2 and CQ suppress large aggregates (Figs. 2 and 3) and appear to induce a low MW species of Aβ at ~1:1 stoichiometry (Figs. 2 and 3). The formation of a stable 8-HQ/Aβ complex, however, was not detected by the NMR experiments (Fig. 7). These results parallel other studies on hydroxyquinoline interactions with Aβ, which have shown that hydroxyquinoline-based compounds can inhibit aggregation (LeVine et al., 2009). In contrast to other studies on PBT2 and CQ interacting with Aβ (Kenche et al., 2013), we show that the interaction can be independent of divalent transition elements. Analysis of our buffers and reagents with ICPMS indicates that divalent metal levels are insignificant ($\ll 0.03 \mu M$) and are not retained with the complex on nitrocellulose (Fig. 5). Further support of this conclusion is provided by the size exclusion results, in which the buffers contained 50 μM EDTA and where the same inhibition of aggregation and stabilization of low MW species was observed as in experiments where EDTA was not present.

There are several toxicity studies, including LTP and mouse cognition studies (Cherny et al., 2001; Adlard et al., 2008), cell and yeast culture studies (Abramov et al., 2003; Tardiff et al.,

elegans (McColl et al., 2012). Consistent with the protective effects of 8-HQ, we determined that CQ was also able to significantly reduce toxicity of human Aβ1–42 expressed in the body wall muscle cells (Fig. 9A). Using a range of concentrations, we observed that 24 h exposure to 30 μM PBT2/CQ provided a robust level of protection against Aβ-induced paralysis. This treatment significantly delays the onset of the toxic phenotype but does not completely prevent it. This indicates that these compounds can only partially rescue Aβ toxicity in this model. Initially, we investigated the effect of 8-HQ compounds on Aβ oligomerization using an ELISA, which uses one antibody to both capture and detect Aβ (W02, epitope: Aβ5–8) (Ida et al., 1996), based on the assumption that only oligomeric forms of Aβ will display a second epitope for W0–2 to bind. The validity of this assumption was determined by comparing the effects of equimolar amounts of preaggregated Aβ (which showed a high response in the assay) against freshly prepared and denatured Aβ, both of which showed no response. Soluble lysates of *C. elegans* treated with PBT2 or CQ had a significant ($p < 0.0001$), but moderate, 20% reduction in the ELISA signal compared with untreated controls (Fig. 9B). Although this was suggestive of an altered oli-

2012; Matlack et al., 2014), and our previous *C. elegans* experiments (McColl et al., 2012), indicating that Aβ toxicity can be attenuated in the presence of PBT2 or CQ. We have reinvestigated the toxicity of Aβ1–42 in the presence of 8-HQ under our experimental conditions (Fig. 8) and have confirmed that the stabilized dimer is nontoxic. Furthermore, our current *C. elegans* results confirm a significant change in the toxic phenotype observed with Aβ expression. The previous *C. elegans* experiments also indicated no significant change in amyloid deposits (McColl et al., 2012), although our current results indicate a significant reduction in oligomeric species. These results are consistent with the current Aβ oligomer hypothesis that oligomeric species of Aβ are toxic and while the amyloid plaques/fibrils are not inherently toxic but a consequence of the aberrant aggregation of Aβ (for review, see Hayden et al., 2013). In particular, our results suggest that high MW (i.e., >20–30 kDa, minimum stoichiometry of a tetramer) oligomers represent the pool of toxic species, whereas low MW oligomers (i.e., dimers) represent a relatively nontoxic form of the peptide. This is consistent with the observation that tetramers may constitute the minimum toxic species (Streltsov et al., 2011). Furthermore, our data support the mechanism that 8-HQ can directly engage Aβ oligomers and monomers to ameliorate the activity of toxic high stoichiometry and MW (>30 kDa) soluble oligomers of Aβ. The previous toxicity (Abramov et al., 2003; Adlard et al., 2008; McColl et al., 2012; Tardiff et al., 2012; Matlack et al., 2014) data in conjunction with our toxicity data (Fig. 8) and characterization of Aβ in the presence of 8-HQ, suggests that these stabilized low MW oligomers are nontoxic. This further indicates that PBT2 and CQ not only stabilize Aβ and suppress aggregation but that these compounds also neutralize large toxic Aβ peptides and oligomers.

In addition to the currently explored mechanisms of action of PBT2 and CQ, we demonstrated that hydroxyquinolines have the capability to directly influence the self-association and *in vivo* toxicity of the Aβ peptide. This activity is complimentary to the other mechanisms of action described for PBT2, and particularly correlates with the disaggregation of amyloid fibrils, inhibition of reactive oxygen species generated by Aβ copper complexes, and inhibition of dityrosine crosslinks. The stabilization of nontoxic Aβ oligomers does not preclude a metal chaperone activity that can occur in the complex biological milieu (Adlard et al., 2008; Crouch et al., 2011) or an ionophoric activity resulting in promotion of intracellular transition metal uptake by neurons. However, these results do indicate that 8-HQ have an additional beneficial mode of action that relates to the formation and degradation of toxic oligomeric species.

These results also raise some interesting questions in regards to what the toxic oligomeric species may be. Our results suggest that 8-HQ-stabilized low MW (dimeric) Aβ oligomers are not toxic, and the observations in the wider literature of a range of oligomers (for review of Aβ oligomerization, see Hayden et al.,
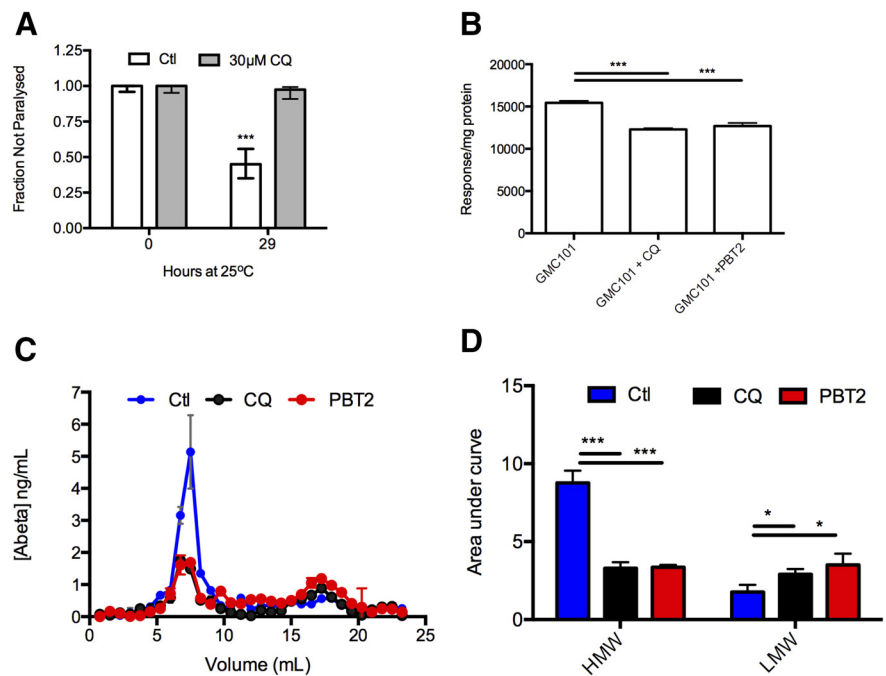
Figure 9. 8-HQs affect Aβ1–42 toxicity in model animals. **A**, The effect of CQ on the paralysis phenotype observed in transgenic *C. elegans*, where the number of animals trialed: $n = 105$ (Ctl) and $n = 108$ (CQ). ***$p < 0.001$. **B**, ELISA quantitation of the oligomeric status of Aβ expressed in soluble lysates derived from *C. elegans* cultured in the absence or presence of 30 μM CQ or PBT2. **C**, Size exclusion (Superdex S75, PBS, 0.75 ml/min) analysis of the oligomeric status of Aβ1–42 in the soluble fraction of lysates from transgenic *C. elegans* cultured in the absence (blue) or presence of 30 μM CQ (black) or PBT2 (red). **D**, Area under curve analysis of the high MW (elution volume ∼5–10 ml) and low MW (elution volume 15–20 ml) Aβ1–42 oligomers. Blue represents transgenic *C. elegans* alone. Black represents CQ-treated transgenic *C. elegans*. Red represents PBT2-treated transgenic *C. elegans*. *$p < 0.05$, ***$p < 0.001$.

2013) having toxic properties suggest that synaptic loss in AD is mediated by not a single oligomeric species, but a range of different oligomers having varying degrees of toxicity, oligomeric status, and solubility. This complexity may preclude identifying a therapy targeted to a specific oligomer; as such, a targeted approach could miss a multitude of other toxic oligomeric species. An alternative to targeting a specific oligomer for neutralization or depletion is to stabilize a native, nontoxic, or nonpathogenic form of the protein/peptide (for review, see Johnson et al., 2012). This approach has been applied with great success to transthyretin (TTR) systemic amyloidosis, where the natively folded TTR tetramer slowly dissociates, generally under the influence of mutation, to misfolded monomeric proteins that rapidly aggregate via an energetically favorable "downhill" polymerization process into amyloid fibrils (Colon and Kelly, 1992; Hurshman et al., 2004; Foss et al., 2005; Johnson et al., 2005). In this pathway, the rate-limiting step is the dissociation of the native tetramer (Foss et al., 2005), and this has led to a significant effort to identify methods to stabilize the native TTR conformation. This research effort identified Tamafidis [2-(3,5-dichloro-phenyl)-benzoxazole-6-carboxylic acid] for the treatment of TTR systemic amyloidosis in familial amyloid neuropathy (Johnson et al., 2012). This compound acts by binding with high specificity and affinity (∼50 nM) to one of the thyroxine binding sites on TTR and stabilizing the dimer–dimer interface of the tetramer through hydrophobic and electrostatic interactions (Bulawa et al., 2012). This prevents the dissociation of the tetramer and thus formation of misfolded monomer and amyloid fibrils (Bulawa et al., 2012). Tafamidis was shown to significantly slow progression of the disease process, including autonomic and peripheral neuropathies,

and improved autonomic nervous system function and cachexia (Coelho et al., 2012, 2013). This efficacy proves the concept that stabilization of a native, stable conformation can have significant outcomes in protein misfolding diseases. Although TTR follows a different pathway from the typical nucleated polymerization (NP) models applied to amyloidogenesis, the activation energy for monomer dissociation is akin to the energy required to form a nucleus in the NP model. This suggests that similar strategies, where a nontoxic conformation is stabilized by the binding of particular compounds, may be applicable to the wider range of amyloid related diseases. In support of this theory, a recent study on the effect of gallic acid interacting with α-synuclein showed that the binding of this compound prevented the collapse of the protein into an aggregation prone form (Liu et al., 2014). Interestingly, this interaction, while having large and significant effects on the biophysics of the protein, also only displayed extremely subtle effects when investigated by NMR (Liu et al., 2014). Our results lend further support to these theories, suggesting that PBT2/CQ variants have an additional mechanism of action whereby Aβ is stabilized in a nontoxic low MW form.

References

Abramov AY, Canevari L, Duchen MR (2003) Changes in intracellular calcium and glutathione in astrocytes as the primary mechanism of amyloid neurotoxicity. J Neurosci 23:5088–5095. Medline

Adlard PA, Cherny RA, Finkelstein DI, Gautier E, Robb E, Cortes M, Volitakis I, Liu X, Smith JP, Perez K, Laughton K, Li QX, Charman SA, Nicolazzo JA, Wilkins S, Deleva K, Lynch T, Kok G, Ritchie CW, Tanzi RE, Cappai R, Masters CL, Barnham KJ, Bush AI (2008) Rapid restoration of cognition in Alzheimer's transgenic mice with 8-hydroxy quinoline analogs is associated with decreased interstitial Abeta. Neuron 59:43–55. CrossRef Medline

Austin C, Hare D, Rozelle AL, Robinson WH, Grimm R, Doble P (2009) Elemental bio-imaging of calcium phosphate crystal deposits in knee samples from arthritic patients. Metallomics 1:142–147. CrossRef Medline

Bailey MF, Angley LM, Perugini MA (2009) Methods for sample labeling and meniscus determination in the fluorescence-detected analytical ultracentrifuge. Anal Biochem 390:218–220. CrossRef Medline

Benilova I, Karran E, De Strooper B (2012) The toxic Abeta oligomer and Alzheimer's disease: an emperor in need of clothes. Nat Neurosci 15:349–357. CrossRef Medline

Bernadó P, Mylonas E, Petoukhov MV, Blackledge M, Svergun DI (2007) Structural characterization of flexible proteins using small-angle X-ray scattering. J Am Chem Soc 129:5656–5664. CrossRef Medline

Brenner S (1974) The genetics of Caenorhabditis elegans. Genetics 77:71–94. Medline

Bulawa CE, Connelly S, Devit M, Wang L, Weigel C, Fleming JA, Packman J, Powers ET, Wiseman RL, Foss TR, Wilson IA, Kelly JW, Labaudinière R (2012) Tafamidis, a potent and selective transthyretin kinetic stabilizer that inhibits the amyloid cascade. Proc Natl Acad Sci U S A 109:9629–9634. CrossRef Medline

Bush AI (2008) Drug development based on the metals hypothesis of Alzheimer's disease. J Alzheimers Dis 15:223–240. Medline

Cheng XR, Sze Hung VW, Scarano S, Mascini M, Minunni M, Kerman K (2012) Label-free methods for probing the interaction of clioquinol with amyloid-[small beta]. Anal Methods 4:2228–2232. CrossRef

Cherny RA, Atwood CS, Xilinas ME, Gray DN, Jones WD, McLean CA, Barnham KJ, Volitakis I, Fraser FW, Kim Y, Huang X, Goldstein LE, Moir RD, Lim JT, Beyreuther K, Zheng H, Tanzi RE, Masters CL, Bush AI (2001) Treatment with a copper-zinc chelator markedly and rapidly inhibits beta-amyloid accumulation in Alzheimer's disease transgenic mice. Neuron 30:665–676. CrossRef Medline

Coelho T, Maia LF, Martins da Silva A, Waddington Cruz M, Planté-Bordeneuve V, Lozeron P, Suhr OB, Campistol JM, Conceiçao IM, Schmidt HH, Trigo P, Kelly JW, Labaudinière R, Chan J, Packman J, Wilson A, Grogan DR (2012) Tafamidis for transthyretin familial amyloid polyneuropathy: a randomized, controlled trial. Neurology 79:785–792. CrossRef Medline

Coelho T, Maia LF, da Silva AM, Cruz MW, Planté-Bordeneuve V, Suhr OB, Conceiçao I, Schmidt HH, Trigo P, Kelly JW, Labaudinière R, Chan J, Packman J, Grogan DR (2013) Long-term effects of tafamidis for the treatment of transthyretin familial amyloid polyneuropathy. J Neurol 260:2802–2814. CrossRef Medline

Colon W, Kelly JW (1992) Partial denaturation of transthyretin is sufficient for amyloid fibril formation in vitro. Biochemistry 31:8654–8660. CrossRef Medline

Crouch PJ, Savva MS, Hung LW, Donnelly PS, Mot AI, Parker SJ, Greenough MA, Volitakis I, Adlard PA, Cherny RA, Masters CL, Bush AI, Barnham KJ, White AR (2011) The Alzheimer's therapeutic PBT2 promotes amyloid-beta degradation and GSK3 phosphorylation via a metal chaperone activity. J Neurochem 119:220–230. CrossRef Medline

Faux NG, Ritchie CW, Gunn A, Rembach A, Tsatsanis A, Bedo J, Harrison J, Lannfelt L, Blennow K, Zetterberg H, Ingelsson M, Masters CL, Tanzi RE, Cummings JL, Herd CM, Bush AI (2010) PBT2 rapidly improves cognition in Alzheimer's disease: additional phase II analyses. J Alzheimers Dis 20:509–516. CrossRef Medline

Foss TR, Wiseman RL, Kelly JW (2005) The pathway by which the tetrameric protein transthyretin dissociates. Biochemistry 44:15525–15533. CrossRef Medline

Franke D, Svergun DI (2009) DAMMIF, a program for rapid ab-initio shape determination in small-angle scattering. J Appl Crystallogr 42:342–346. CrossRef

Hare DJ, George JL, Grimm R, Wilkins S, Adlard PA, Cherny RA, Bush AI, Finkelstein DI, Doble P (2010) Three-dimensional elemental bio-imaging of Fe, Zn, Cu, Mn and P in a 6-hydroxydopamine lesioned mouse brain. Metallomics 2:745–753. CrossRef Medline

Hare DJ, Grubman A, Ryan TM, Lothian A, Liddell JR, Grimm R, Matsuda T, Doble PA, Cherny RA, Bush AI, White AR, Masters CL, Roberts BR (2013) Profiling the iron, copper and zinc content in primary neuron and astrocyte cultures by rapid online quantitative size exclusion chromatography-inductively coupled plasma-mass spectrometry. Metallomics 5:1656–1662. CrossRef Medline

Hare DJ, Lee JK, Beavis AD, van Gramberg A, George J, Adlard PA, Finkelstein DI, Doble PA (2012) Three-dimensional atlas of iron, copper, and zinc in the mouse cerebrum and brainstem. Anal Chem 84:3990–3997. CrossRef Medline

Hayden EY, Teplow DB (2013) Amyloid beta-protein oligomers and Alzheimer's disease. Alzheimers Res Ther 5:60. CrossRef Medline

Hurshman AR, White JT, Powers ET, Kelly JW (2004) Transthyretin aggregation under partially denaturing conditions is a downhill polymerization. Biochemistry 43:7365–7381. CrossRef Medline

Ida N, Hartmann T, Pantel J, Schröder J, Zerfass R, Förstl H, Sandbrink R, Masters CL, Beyreuther K (1996) Analysis of heterogeneous A4 peptides in human cerebrospinal fluid and blood by a newly developed sensitive Western blot assay. J Biol Chem 271:22908–22914. CrossRef Medline

Imbimbo BP, Ottonello S, Frisardi V, Solfrizzi V, Greco A, Seripa D, Pilotto A, Panza F (2012) Solanezumab for the treatment of mild-to-moderate Alzheimer's disease. Expert Rev Clin Immunol 8:135–149. CrossRef Medline

Johnson SM, Connelly S, Fearns C, Powers ET, Kelly JW (2012) The transthyretin amyloidoses: from delineating the molecular mechanism of aggregation linked to pathology to a regulatory-agency-approved drug. J Mol Biol 421:185–203. CrossRef Medline

Johnson SM, Wiseman RL, Sekijima Y, Green NS, Adamski-Werner SL, Kelly JW (2005) Native state kinetic stabilization as a strategy to ameliorate protein misfolding diseases: a focus on the transthyretin amyloidoses. Acc Chem Res 38:911–921. CrossRef Medline

Kang J, Lemaire HG, Unterbeck A, Salbaum JM, Masters CL, Grzeschik KH, Multhaup G, Beyreuther K, Müller-Hill B (1987) The precursor of Alzheimer's disease amyloid A4 protein resembles a cell-surface receptor. Nature 325:733–736. CrossRef Medline

Kenche VB, Zawisza I, Masters CL, Bal W, Barnham KJ, Drew SC (2013) Mixed ligand Cu^{2+} complexes of a model therapeutic with Alzheimer's amyloid-beta peptide and monoamine neurotransmitters. Inorg Chem 52:4303–4318. CrossRef Medline

Kirby NM, Mudie ST, Hawley AM, Cookson DJ, Mertens HDT, Cowieson N, Samardzic-Boban V (2013) A low-background-intensity focusing small-angle X-ray scattering undulator beamline. J Appl Crystallogr 46:1670–1680. CrossRef

Kohn JE, Millett IS, Jacob J, Zagrovic B, Dillon TM, Cingel N, Dothager RS,

Seifert S, Thiyagarajan P, Sosnick TR, Hasan MZ, Pande VS, Ruczinski I, Doniach S, Plaxco KW (2004) Random-coil behavior and the dimensions of chemically unfolded proteins. Proc Natl Acad Sci U S A 101: 12491–12496. CrossRef Medline

Konarev PV, Volkov VV, Sokolova AV, Koch MHJ, Svergun DI (2003) PRIMUS: a Windows PC-based system for small-angle scattering data analysis. J Appl Crystallogr 36:1277–1282. CrossRef

Lambert MP, Barlow AK, Chromy BA, Edwards C, Freed R, Liosatos M, Morgan TE, Rozovsky I, Trommer B, Viola KL, Wals P, Zhang C, Finch CE, Krafft GA, Klein WL (1998) Diffusible, nonfibrillar ligands derived from Abeta1–42 are potent central nervous system neurotoxins. Proc Natl Acad Sci U S A 95:6448–6453. CrossRef Medline

Lannfelt L, Blennow K, Zetterberg H, Batsman S, Ames D, Harrison J, Masters CL, Targum S, Bush AI, Murdoch R, Wilson J, Ritchie CW (2008) Safety, efficacy, and biomarker findings of PBT2 in targeting Abeta as a modifying therapy for Alzheimer's disease: a phase IIa, double-blind, randomised, placebo-controlled trial. Lancet Neurol 7:779–786. CrossRef Medline

Lear J, Hare DJ, Fryer F, Adlard PA, Finkelstein DI, Doble PA (2012) High-resolution elemental bioimaging of Ca, Mn, Fe, Co, Cu, and Zn employing LA-ICPMS and hydrogen reaction gas. Anal Chem 84:6707–6714. CrossRef Medline

Lesné S, Koh MT, Kotilinek L, Kayed R, Glabe CG, Yang A, Gallagher M, Ashe KH (2006) A specific amyloid-beta protein assembly in the brain impairs memory. Nature 440:352–357. CrossRef Medline

LeVine H 3rd, Ding Q, Walker JA, Voss RS, Augelli-Szafran CE (2009) Clioquinol and other hydroxyquinoline derivatives inhibit Abeta(1–42) oligomer assembly. Neurosci Lett 465:99–103. CrossRef Medline

Lim NK, Villemagne VL, Soon CP, Laughton KM, Rowe CC, McLean CA, Masters CL, Evin G, Li QX (2011) Investigation of matrix metalloproteinases, MMP-2 and MMP-9, in plasma reveals a decrease of MMP-2 in Alzheimer's disease. J Alzheimers Dis 26:779–786. CrossRef Medline

Liu Y, Carver JA, Calabrese AN, Pukala TL (2014) Gallic acid interacts with alpha-synuclein to prevent the structural collapse necessary for its aggregation. Biochim Biophys Acta 1844:1481–1485. CrossRef Medline

Masters CL, Simms G, Weinman NA, Multhaup G, McDonald BL, Beyreuther K (1985) Amyloid plaque core protein in Alzheimer disease and Down syndrome. Proc Natl Acad Sci U S A 82:4245–4249. CrossRef Medline

Matlack KE, Tardiff DF, Narayan P, Hamamichi S, Caldwell KA, Caldwell GA, Lindquist S (2014) Clioquinol promotes the degradation of metal-dependent amyloid-beta (Abeta) oligomers to restore endocytosis and ameliorate Abeta toxicity. Proc Natl Acad Sci U S A 111:4013–4018. CrossRef Medline

Mawuenyega KG, Sigurdson W, Ovod V, Munsell L, Kasten T, Morris JC, Yarasheski KE, Bateman RJ (2010) Decreased clearance of CNS beta-amyloid in Alzheimer's disease. Science 330:1774. CrossRef Medline

McColl G, Roberts BR, Gunn AP, Perez KA, Tew DJ, Masters CL, Barnham KJ, Cherny RA, Bush AI (2009) The *Caenorhabditis elegans* A beta 1–42 model of Alzheimer disease predominantly expresses A beta 3–42. J Biol Chem 284:22697–22702. CrossRef Medline

McColl G, Roberts BR, Pukala TL, Kenche VB, Roberts CM, Link CD, Ryan TM, Masters CL, Barnham KJ, Bush AI, Cherny RA (2012) Utility of an improved model of amyloid-beta (Abeta1–42) toxicity in *Caenorhabditis elegans* for drug screening for Alzheimer's disease. Mol Neurodegener 7:57. CrossRef Medline

Mok YF, Ryan TM, Yang S, Hatters DM, Howlett GJ, Griffin MD (2011) Sedimentation velocity analysis of amyloid oligomers and fibrils using fluorescence detection. Methods 54:67–75. CrossRef Medline

Opazo C, Luza S, Villemagne VL, Volitakis I, Rowe C, Barnham KJ, Strozyk D, Masters CL, Cherny RA, Bush AI (2006) Radioiodinated clioquinol as a biomarker for beta-amyloid: Zn complexes in Alzheimer's disease. Aging Cell 5:69–79. CrossRef Medline

Padmanabhan G, Becue I, Smith J (1989) Clioquinol. In: Analytical profiles of drug substances (Klauss E, Florey E, eds). San Diego: Academic.

Petoukhov MV, Franke D, Shkumatov AV, Tria G, Kikhney AG, Gajda M, Gorba C, Mertens HD, Konarev PV, Svergun DI (2012) New developments in the ATSAS program package for small-angle scattering data analysis. J Appl Crystallogr 45:342–350. CrossRef Medline

Petoukhov MV, Konarev PV, Kikhney AG, Svergun DI (2007) ATSAS 2.1: towards automated and web-supported small-angle scattering data analysis. J Appl Crystallogr 40 [Suppl]:S223–S228.

Rembach A, Hare DJ, Doecke JD, Burnham SC, Volitakis I, Fowler CJ, Cherny RA, McLean C, Grimm R, Martins R, Ames D, Masters CL, Bush AI, Roberts BR (2014) Decreased serum zinc is an effect of ageing and not Alzheimer's disease. Metallomics 6:1216–1219. CrossRef Medline

Ryan TM, Caine J, Mertens HD, Kirby N, Nigro J, Breheney K, Waddington LJ, Streltsov VA, Curtain C, Masters CL, Roberts BR (2013a) Ammonium hydroxide treatment of Abeta produces an aggregate free solution suitable for biophysical and cell culture characterization. PeerJ 1:e73. CrossRef Medline

Ryan TM, Friedhuber A, Lind M, Howlett GJ, Masters C, Roberts BR (2012) Small amphipathic molecules modulate secondary structure and amyloid fibril-forming kinetics of Alzheimer disease peptide Abeta(1–42). J Biol Chem 287:16947–16954. CrossRef Medline

Ryan TM, Griffin MD, Bailey MF, Schuck P, Howlett GJ (2011) NBD-labeled phospholipid accelerates apolipoprotein C-II amyloid fibril formation but is not incorporated into mature fibrils. Biochemistry 50: 9579–9586. CrossRef Medline

Ryan TM, Roberts BR, Streltsov VA, Nuttall SD, Masters CL (2013b) The role of Aβ in Alzheimer's disease: amyloid fibrils and prefibrillar aggregates. New York: Wiley-VCH Verlag.

Schuck P (2000) Size-distribution analysis of macromolecules by sedimentation velocity ultracentrifugation and lamm equation modeling. Biophys J 78:1606–1619. CrossRef Medline

Schuck P (2003) On the analysis of protein self-association by sedimentation velocity analytical ultracentrifugation. Anal Biochem 320:104–124. CrossRef Medline

Shankar GM, Li S, Mehta TH, Garcia-Munoz A, Shepardson NE, Smith I, Brett FM, Farrell MA, Rowan MJ, Lemere CA, Regan CM, Walsh DM, Sabatini BL, Selkoe DJ (2008) Amyloid-beta protein dimers isolated directly from Alzheimer's brains impair synaptic plasticity and memory. Nat Med 14:837–842. CrossRef Medline

Streltsov VA, Varghese JN, Masters CL, Nuttall SD (2011) Crystal structure of the amyloid-beta p3 fragment provides a model for oligomer formation in Alzheimer's disease. J Neurosci 31:1419–1426. CrossRef Medline

Svergun ND (1992) Determination of the regularization parameter in indirect-transform methods using perceptual criteria. J Appl Crystallogr 25:495–503. CrossRef

Tardiff DF, Tucci ML, Caldwell KA, Caldwell GA, Lindquist S (2012) Different 8-hydroxyquinolines protect models of TDP-43 protein, alpha-synuclein, and polyglutamine proteotoxicity through distinct mechanisms. J Biol Chem 287:4107–4120. CrossRef Medline

Tayeb HO, Murray ED, Price BH, Tarazi FI (2013) Bapineuzumab and solanezumab for Alzheimer's disease: is the 'amyloid cascade hypothesis' still alive? Expert Opin Biol Ther 13:1075–1084. CrossRef Medline

Telpoukhovskaia MA, Rodríguez-Rodríguez C, Cawthray JF, Scott LE, Page BD, Alí-Torres J, Sodupe M, Bailey GA, Patrick BO, Orvig C (2014) 3-Hydroxy-4-pyridinone derivatives as metal ion and amyloid binding agents. Metallomics 6:249–262. CrossRef Medline

Vistica J, Dam J, Balbo A, Yikilmaz E, Mariuzza RA, Rouault TA, Schuck P (2004) Sedimentation equilibrium analysis of protein interactions with global implicit mass conservation constraints and systematic noise decomposition. Anal Biochem 326:234–256. CrossRef Medline

White AR, Du T, Laughton KM, Volitakis I, Sharples RA, Xilinas ME, Hoke DE, Holsinger RM, Evin G, Cherny RA, Hill AF, Barnham KJ, Li QX, Bush AI, Masters CL (2006) Degradation of the Alzheimer disease amyloid beta-peptide by metal-dependent up-regulation of metalloprotease activity. J Biol Chem 281:17670–17680. CrossRef Medline

Author/s:
Ryan, TM; Roberts, BR; McColl, G; Hare, DJ; Doble, PA; Li, Q-X; Lind, M; Roberts, AM; Mertens, HDT; Kirby, N; Pham, CLL; Hinds, MG; Adlard, PA; Barnham, KJ; Curtain, CC; Masters, CL

Title:
Stabilization of Nontoxic A beta-Oligomers: Insights into the Mechanism of Action of Hydroxyquinolines in Alzheimer's Disease

Date:
2015-02-18

Citation:
Ryan, T. M., Roberts, B. R., McColl, G., Hare, D. J., Doble, P. A., Li, Q. -X., Lind, M., Roberts, A. M., Mertens, H. D. T., Kirby, N., Pham, C. L. L., Hinds, M. G., Adlard, P. A., Barnham, K. J., Curtain, C. C. & Masters, C. L. (2015). Stabilization of Nontoxic A beta-Oligomers: Insights into the Mechanism of Action of Hydroxyquinolines in Alzheimer's Disease. JOURNAL OF NEUROSCIENCE, 35 (7), pp.2871-2884. https://doi.org/10.1523/JNEUROSCI.2912-14.2015.

Persistent Link:
http://hdl.handle.net/11343/59261

File Description:
Published version